

Preconditioned One-Step Generative Modeling for Bayesian Inverse Problems in Function Spaces

Zilan Cheng*

Li-Lian Wang[†]

Zhongjian Wang[‡]

March 17, 2026

Abstract

We propose a machine-learning algorithm for Bayesian inverse problems in the function-space regime based on one-step generative transport. Building on the Mean Flows, we learn a fully conditional amortized sampler with a neural-operator backbone that maps a reference Gaussian noise to approximate posterior samples. We show that while white-noise references may be admissible at fixed discretization, they become incompatible with the function-space limit, leading to instability in inference for Bayesian problems arising from PDEs. To address this issue, we adopt a prior-aligned anisotropic Gaussian reference distribution and establish the Lipschitz regularity of the resulting transport. Our method is not distilled from MCMC: training relies only on prior samples and simulated partial and noisy observations. Once trained, it generates a 64×64 posterior sample in $\sim 10^{-3}$ s, avoiding the repeated PDE solves of MCMC while matching key posterior summaries.

1 Introduction

Bayesian inference provides a principled framework for uncertainty quantification in scientific computing [27, 6], characterizing uncertainty induced by noisy, incomplete, or indirect observations. This paradigm underpins uncertainty-aware prediction and decision-making across a wide range of applications, including porous media [14], imaging [29], geophysics [22], structural model updating [2], and model calibration [15]. This perspective is particularly important for inverse problems governed by partial differential equations (PDEs), where unknowns are functions such as coefficients, source terms, or initial conditions; and observational and modeling bias are unavoidable. In such settings, posterior distributions are typically high- or infinite-dimensional, and efficient sampling methods are central to practical Bayesian inversion.

Classical sampling methods for Bayesian inverse problems, most notably Markov chain Monte Carlo (MCMC), are theoretically well understood and asymptotically exact. A key insight from the function-space theory is that sampling efficiency depends crucially on the geometry of the prior and posterior measures. In particular, preconditioned samplers—such as the preconditioned Crank–Nicolson (pCN) algorithm—replace white-noise random-walk proposals by Gaussian perturbations aligned with the prior covariance, yielding dimension-robust behavior and making them a cornerstone of modern Bayesian inversion [27, 5]. Nevertheless, these methods rely on long correlated chains and repeated forward solves, and can be prohibitively expensive in practice for large-scale PDE inverse problems (see Section 4 for runtime comparisons).

*Division of Mathematical Sciences, School of Physical and Mathematical Sciences, Nanyang Technological University, 637371, Singapore. Email: zilan001@e.ntu.edu.sg.

[†]Division of Mathematical Sciences, School of Physical and Mathematical Sciences, Nanyang Technological University, 637371, Singapore. Email: lilian@ntu.edu.sg.

[‡]Corresponding author. Division of Mathematical Sciences, School of Physical and Mathematical Sciences, Nanyang Technological University, 637371, Singapore. Email: zhongjian.wang@ntu.edu.sg.

In machine learning, generative models are used to generate samples by probing the target distribution from data. Among them, the diffusion and score-based generative models may serve as an *amortized samplers* for Bayesian inverse problems: they learn a transport from a simple reference distribution to (an approximation of) the posterior and draw samples by simulating the learned dynamics [12, 26, 3, 17]. Closely related, flow matching learns the associated transport velocity field directly, offering an ODE/continuous-flow viewpoint [18, 1, 19].

A practical limitation of these multi-step approaches is that inference cost typically scales with the number of integration steps. More recently, *Mean Flows* [9, 10] introduce a *one-step* transport alternative, enabling sample generation without long SDE/ODE integration at inference time. Building on Mean Flows generative backbone, we develop a *fully conditional* operator model that maps a reference draw to an approximate posterior sample, enabling *single-pass* inference for PDE inverse problems.

Concretely, we seek to infer an unknown field x endowed with a prior γ from partial noisy observations

$$x \sim \gamma, y_{\text{obs}} = \mathcal{O}(\mathcal{G}(x)) + \eta, \eta \sim \mathcal{N}(0, \sigma_\eta^2 I), \quad (1)$$

where \mathcal{G} denotes the forward (typically PDE) map, \mathcal{O} the observation operator, and η measurement noise. Given y_{obs} , our model learns a conditional transport $\mathcal{T}_\theta(\cdot; y_{\text{obs}})$ that turns a draw ξ from an easy-to-sample base measure ρ into an approximate posterior sample $\pi(\cdot | y_{\text{obs}})$ (see Figure 2 for a road map).

To build intuition, we begin with a simple but revealing identity inverse problem where $\mathcal{G} = I : x \mapsto (x(p))_{p \in P}$ with P denoting a set of 49 *randomly* selected observation points in the domain $\Omega = [0, 1]^2$. Under the Bayesian setting, we consider a trace-class anisotropic prior $x \sim \mathcal{N}(0, (-\Delta + 9I)^{-2})$ where Δ denotes the Laplacian operator with Neumann boundary condition on Ω . The additive observation noise η is assumed following $\mathcal{N}(0, 0.1^2 I)$. The generative task in such a Bayesian setting is then to generate a distribution conditioned on y_{obs} , equivalently, the posterior distribution. Therefore, one may apply any off-the-shelf diffusion model to the data generated by (1). For illustration, we repeat the experiment under various design choices in terms of spatial discretization, reference distribution of the diffusion model, and normalization encoding structure.

Figure 1 reports the 10^3 -sample averaged energy spectra of model-generated posterior samples under two training protocols: our main *Encode-only* setting (Algorithms 1–2), and an *Encode–Decode* variant (Algorithms 3–4). In each case, the sampler is driven either by a white-noise reference ρ_W or by a trace-class anisotropic reference $\rho_A = \gamma$ aligned with the prior. The resulting radially averaged energy spectra are compared against the closed-form posterior π_{exact} (derived in Appendix A.1) as well as the prior γ :

$$E(k) := \frac{1}{|\mathcal{S}_k|} \sum_{(k_1, k_2) \in \mathcal{S}_k} \left(\frac{1}{10^3} \sum_{j=1}^{10^3} |\hat{x}_{k_1, k_2}^{(j)}|^2 \right),$$

$$\mathcal{S}_k := \left\{ (k_1, k_2) : k - \frac{1}{2} \leq \sqrt{k_1^2 + k_2^2} < k + \frac{1}{2} \right\},$$

Even when L^2 errors might be comparable at a fixed discretization (Table 2) in Encode-only setting, the spectra reveal qualitative differences: on the finer grid, ρ_W exhibits clear high-frequency deviations, and this effect is markedly amplified in the Encode–Decode variant. By contrast, using a prior-matched trace-class reference produces spectra that closely track π_{exact} and preserves the correct spectral decay across both training protocols. The identity experiment serves as a diagnostic in the function-space regime, isolating how the reference measure and training space govern dimension-dependent artifacts. This motivates our design and we summarize our contribution of the work as follows:

- Operator learning for amortized conditional generation: we aim to learn a conditional map in function space, namely $(\xi, y_{\text{obs}}) \mapsto \mathcal{T}_\theta(\xi; y_{\text{obs}})$ from prior simulation pairs (x, y_{obs}) . Once

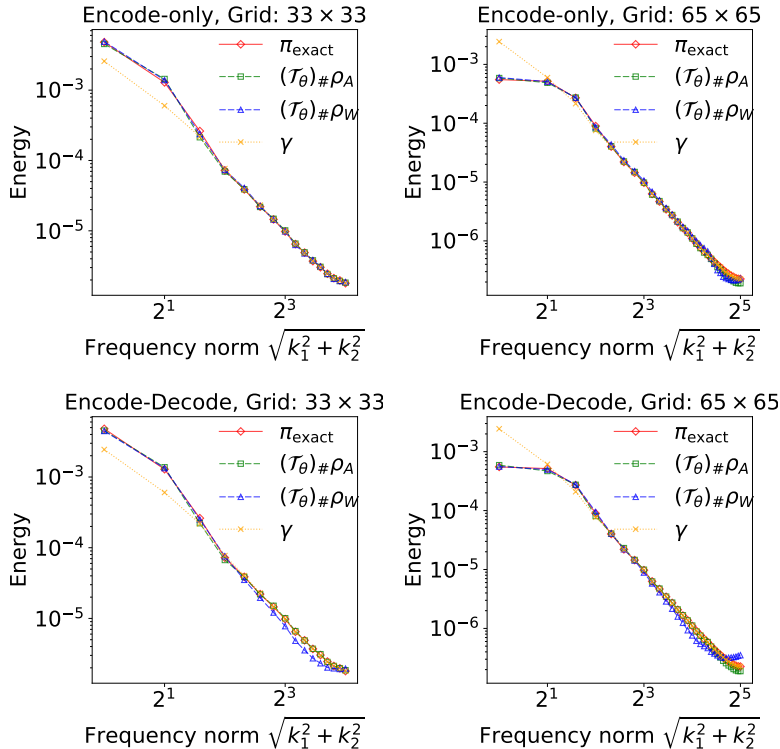


Figure 1: Energy spectra $E(k)$ for the identity inverse problem. Top: Encode-only training (loss in encoded space). Bottom: Encode-Decode training (loss in physical space). For reference, we also plot the ground-truth closed-form posterior π_{exact} (Appendix A.1) and the prior spectrum. The curves labeled $(\mathcal{T}_\theta)\#\rho_A$ and $(\mathcal{T}_\theta)\#\rho_W$ denote model-approximated posteriors obtained by transporting the anisotropic reference $\rho_A = \gamma$ and the white-noise reference ρ_W , respectively, where γ is the trace-class prior.

trained, the same operator *generalizes across observations*: for any new y_{obs} , it produces posterior samples with the same model \mathcal{T}_θ .

- One-step posterior sampling: our generation of posterior is through a one-step transport model. This will largely shorten the inference time compared to conventional multi-step (diffusion) models and trustworthy MCMC solvers.
- Reference measure principle: we justified the necessity of a prior-aligned trace-class base measures to ensure the well-posedness in function space while white noise is not; *Encode-only* acts as a finite-resolution preconditioner that can temporarily mask this issue.

The rest of the paper is organized as follows. Section 2 reviews related work. Section 3 presents the algorithm and theoretical guarantees. Section 4 provides numerical experiments on various PDE-based inverse problems. Section 5 provides conclusive remarks.

2 Related work

2.1 Generative models in forward and inverse problems

Diffusion and flow-matching approaches [12, 26, 18, 1, 19] have become standard paradigms for generative modeling. More recently, Mean Flows [9, 10] were proposed as a *generative modeling paradigm* that enables one-step generation, avoiding long SDE/ODE integration at inference time.

Most generative models are originally developed for prior modeling [7]. Despite this, generative models have increasingly been adapted to perform Bayesian posterior sampling; however, many

works still rely on unconditional training and enforce measurement constraints only at sampling time via data-consistency or guidance-type updates [25, 8]. There are also approaches with conditional training, but they often focus on MAP-style reconstruction / point estimation [28], rather than learning and sampling an explicit posterior distribution.

2.2 Generative models in function-space settings

There is a growing interest in pushing generative models toward function-space formulations, especially for PDE systems. Many existing works still operate after discretization and use finite-dimensional backbones (e.g., UNet-style architectures) [13, 24], often relying on test-time guidance to incorporate observations. Some recent methods extend diffusion/score modeling more explicitly to function space and consider conditional generation [17], but conditional sampling is typically still carried out through multi-step procedures. In the function-space regime, one-step conditional generative modeling remains comparatively under-explored.

2.3 Operator learning

Neural operators (e.g., DeepONet [21], FNO and its variants [16, 20, 4]) provide a natural framework for learning function-to-function mappings and have been widely used as data-driven fast solvers of PDEs (forward model). While they have been combined with iterative generative samplers in some works [17], *one-step conditional* generation for PDE inverse problems remains relatively under-explored. Neural-operator backbones therefore offer a natural route to one-step amortized posterior sampling in function spaces.

3 Main results

In this section, we list the main results: from setting up a Bayesian inverse problem to a one-step posterior sampler.

3.1 Problem setting and objective

Let \mathcal{H} be a separable Hilbert space and interpret the unknown $x \in \mathcal{H}$ as a function-valued quantity (e.g., a PDE coefficient, source term, or initial condition). Let $\mathcal{G} : \mathcal{H} \rightarrow \mathcal{Y}$ be a (possibly nonlinear) PDE forward operator and $\mathcal{O} : \mathcal{Y} \rightarrow \mathbb{R}^m$ a finite-dimensional observation operator. We consider

$$y_{\text{obs}} := \mathcal{G}_{\text{obs}}(x) + \eta = \mathcal{O}(\mathcal{G}(x)) + \eta, \quad x \in \mathcal{H}, \quad y_{\text{obs}} \in \mathbb{R}^m,$$

where $\mathcal{G}_{\text{obs}} : \mathcal{H} \rightarrow \mathbb{R}^m$ denotes the composition of the PDE map and sensor restriction, and $\eta \sim \mathcal{N}(0, \sigma_\eta^2 I_m)$ is additive Gaussian noise.

We adopt an anisotropic Gaussian Bayesian prior $\gamma = \mathcal{N}(0, C)$ on \mathcal{H} (throughout this manuscript, we take $C = (-\Delta + \kappa^2 I)^{-d}$ as a representative example). Given partial noisy observations y_{obs} , the posterior measure is

$$\begin{aligned} \pi(\mathrm{d}x \mid y_{\text{obs}}) &\propto \exp(-\Phi(x; y_{\text{obs}})) \gamma(\mathrm{d}x), \\ \Phi(x; y_{\text{obs}}) &= \frac{1}{2\sigma_\eta^2} \|y_{\text{obs}} - \mathcal{G}_{\text{obs}}(x)\|_2^2. \end{aligned} \tag{2}$$

Under the additive Gaussian noise model, $\Phi \geq 0$ and hence $\exp(-\Phi) \leq 1$, so any Gaussian-tail (exponential integrability) property enjoyed by the trace-class prior γ is inherited by the posterior.

Our objective is to learn a *parametric* transport map conditional on y_{obs} $\mathcal{T}_\theta(\cdot; y_{\text{obs}}) : \mathcal{H} \rightarrow \mathcal{H}$ whose pushforward approximates the posterior:

$$(\mathcal{T}_\theta(\cdot; y_{\text{obs}}))_{\#} \rho \approx \pi(\cdot \mid y_{\text{obs}}),$$

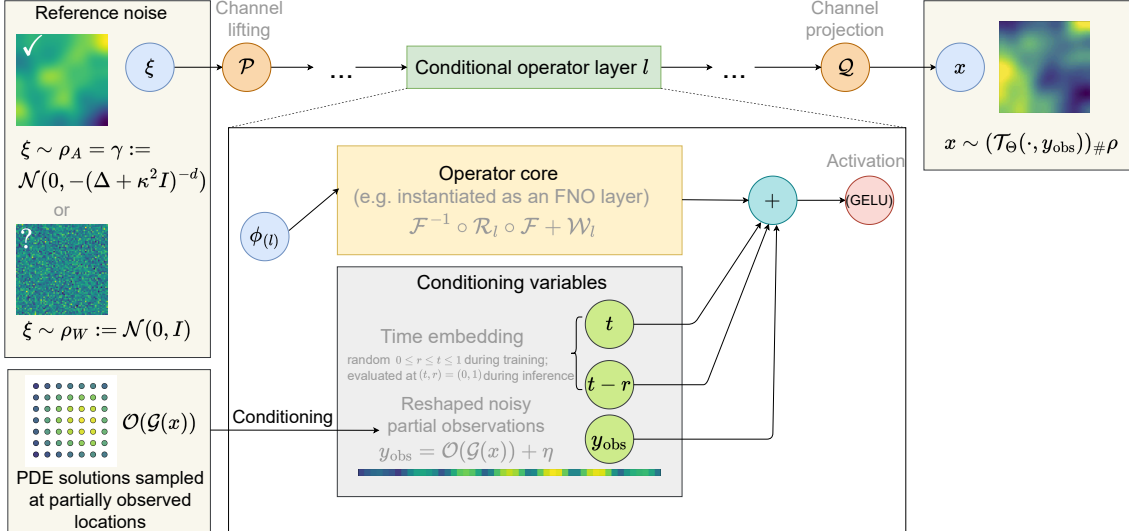


Figure 2: Conditional neural operator backbone for one-step posterior sampling. A latent/reference draw $\xi \sim \rho$ (with $\rho = \gamma$) in our main prior-aligned trace-class setting) is mapped by a lifting operator \mathcal{P} , L conditional operator layers, and a projection operator \mathcal{Q} . During training we sample time pairs $0 \leq r \leq t \leq 1$; at inference we evaluate the learned map at $(r, t) = (0, 1)$ to obtain a one-step transport that generates approximate posterior samples.

where ρ denotes the reference (latent) measure. Here \mathcal{T}_θ is a learned surrogate rather than an exact map. Crucially, θ is shared across all instances: at test time, we simply change y_{obs} and evaluate the same operator model, without any re-training or instance-specific optimization.

Moreover, the model is *fully conditional on y_{obs} only*. No ground-truth posterior samples and no auxiliary *teacher* (e.g., MCMC, diffusion, or any pre-trained sampler) are required: the conditional transport is learned directly from (x, y_{obs}) data.

In our main setting, we adopt a prior-aligned choice $\rho_A = \gamma$, so posterior sampling is performed by a single network evaluation,

$$x = \mathcal{T}_\theta(\xi; y_{\text{obs}}), \quad \xi \sim \gamma,$$

while we also consider discretization-level white-noise latents as baselines. The function-space implications of these choices are analyzed in Section 3.5 and validated numerically in Section 4 and Appendix D.

3.2 Generative backbone: one-step Mean Flows transport

Mean Flows [9] learns a one-step transport by regressing an average velocity along a simple interpolation path that couples a target sample x with an independent reference draw ξ . Let (x, y_{obs}) be drawn from the joint distribution induced by the Bayesian model (i.e., x is a ground-truth latent with corresponding observations y_{obs}), and draw an independent $\xi \sim \rho$, where ρ denotes the reference/latent measure (in our main setting, $\rho = \gamma$).

Consider the linear interpolation and corresponding instantaneous velocity:

$$z_t = (1 - t)x + t\xi, \quad v(z_t, t) = \xi - x, \quad t \in [0, 1]. \quad (3)$$

Mean Flow defines the average velocity $w_{r,t}$ as

$$\begin{aligned} w_{r,t} &:= \frac{1}{t - r} \int_r^t v(z_\tau, \tau) d\tau \\ &= v(z_t, t) - (t - r) \frac{d}{dt} u(z_t, r, t). \end{aligned} \quad (4)$$

We extend the original unconditional model to an observation-conditioned operator that takes the current state $z = z_t$ and the time pair (r, t) as inputs,

$$w_\theta : \mathcal{H} \times [0, 1] \times [0, 1] \times \mathbb{R}^m \rightarrow \mathcal{H},$$

$$(z, r, t, y_{\text{obs}}) \mapsto w_\theta(z, r, t; y_{\text{obs}}),$$

and is trained to approximate the mean-flow velocity $w_{r,t}$ in (4). The resulting one-step sampler evaluates the model at $(r, t) = (0, 1)$ (so that $z_1 = \xi$) and outputs

$$\mathcal{T}_\theta(\xi; y_{\text{obs}}) := \xi - w_\theta(\xi, 0, 1; y_{\text{obs}}), \quad \xi \sim \rho.$$

3.3 Conditional neural operator backbone

We parameterize w_θ as a conditional neural operator (Figure 2). Given a latent/reference draw $\xi \sim \rho$ (in our main setting, $\rho = \gamma$), we form the state z at which the velocity is evaluated (e.g., $z = z_t$ or $z = \xi$ for the one-step sampler), lift z to a feature space via an encoder \mathcal{P} , apply L conditional operator blocks, and project back to \mathcal{H} via a decoder \mathcal{Q} . Concretely, an FNO-style block can be taken as

$$\psi_{\ell+1} = \mathcal{F}^{-1}(\mathcal{R}_\ell(\mathcal{F}\psi_\ell)) + \mathcal{W}_\ell\psi_\ell + \mathcal{I}_\ell(t, t-r, y_{\text{obs}}),$$

where \mathcal{F} denotes the Fourier transform on the spatial grid, \mathcal{R}_ℓ is a learned spectral multiplier (acting on truncated Fourier modes), and \mathcal{W}_ℓ is a local pointwise linear map.

The injection term $\mathcal{I}_\ell(t, t-r, y_{\text{obs}})$ incorporates conditioning information by combining embeddings of the time variables $(t, t-r)$ with an embedding of the (noisy) observations y_{obs} , reshaped onto the spatial grid, and adding the result to the hidden features at each layer.

Algorithm 1 Training: Encode-only Mean Flows

Input: Training pairs $\{(x^{(i)}, y_{\text{obs}}^{(i)})\}_{i=1}^{N_{\text{train}}}$; reference/latent measure ρ (prior-aligned $\rho = \gamma$ in our main setting).

Preprocessing:

Estimate normalization statistics (μ_x, σ_x) and (μ_y, σ_y) from the training set, and define encoders $\tilde{y}_{\text{obs}} = \mathcal{E}_y(y_{\text{obs}})$ in (5) and $\tilde{x} = \mathcal{E}_x(x)$ in (6).

Initialize: network parameters θ .

repeat

Sample a mini-batch (x, y_{obs}) from the training set.

Encode $\tilde{x} = \mathcal{E}_x(x)$ and $\tilde{y}_{\text{obs}} = \mathcal{E}_y(y_{\text{obs}})$.

Sample $\xi \sim \rho$ independently.

Sample (r, t) with $0 \leq r \leq t \leq 1$.

Form the interpolation state $z_t = (1-t)\tilde{x} + t\xi$.

Predict the averaged velocity: $w_\theta(z_t, r, t; \tilde{y}_{\text{obs}})$.

Set the (stop-gradient) regression target (7):

Update θ by minimizing

$$\|w_\theta(z_t, r, t; \tilde{y}_{\text{obs}}) - \text{sg}(w_{\text{tgt}})\|^2.$$

until convergence

Output: trained parameters $\hat{\theta}$.

3.4 Training objectives

We train an averaged-velocity network w_θ using an *encode-only* conditional pipeline. Fix a reference measure ρ (prior-aligned $\rho = \gamma$ in our main setting, and a white-noise baseline $\rho = \rho_W$). Given a training pair (x, y_{obs}) , we first apply a normalization matched to the chosen reference geometry:

Algorithm 2 Sampling: One-step Encode-only Mean Flows

Input: Observation y_{obs} ; trained parameters $\hat{\theta}$; reference/latent measure ρ ; normalizers $\mathcal{E}_x, \mathcal{E}_y$.
 Encode observation $\tilde{y}_{\text{obs}} = \mathcal{E}_y(y_{\text{obs}})$.

Sample $\xi \sim \rho$.

Generate an encoded sample:

$$\tilde{x} = \xi - w_{\hat{\theta}}(\xi, 0, 1; \tilde{y}_{\text{obs}}).$$

Decode to physical space: $x = \mathcal{E}_x^{-1}(\tilde{x})$.

Output: Posterior sample x .

$$\tilde{y}_{\text{obs}} = \mathcal{E}_y(y_{\text{obs}}) = \frac{y_{\text{obs}} - \mu_y}{\sigma_y} \quad (5)$$

$$\tilde{x} = \mathcal{E}_x(x) = \begin{cases} x - \mu_x, & \text{if } \rho = \gamma, \\ \frac{x - \mu_x}{\sigma_x}, & \text{if } \rho = \rho_W, \end{cases} \quad (6)$$

where (μ_x, σ_x) and (μ_y, σ_y) are estimated from the training set.

Remark 3.1 (Normalizer). The state normalizer \mathcal{E}_x should respect the reference geometry. For an anisotropic reference $\rho = \gamma$, a unit-Gaussian (pointwise) normalizer erases the correlation structure and distorts the intended trace-class C -geometry. In contrast, for a discretization-level white reference ρ_W , a unit-Gaussian normalizer acts as a whitening step in the encoded coordinates and can mitigate the white-vs-trace-class mismatch. This is an engineering, discretization-dependent effect and does not remove the intrinsic function-space obstruction (Section 3.5 and Appendix C).

We then draw an independent reference sample $\xi \sim \rho$ and sample times $0 \leq r \leq t \leq 1$. The encoded coupling is:

$$z_t = (1 - t)\tilde{x} + t\xi, \quad v = \xi - \tilde{x}.$$

and predicts the averaged velocity $w_{\theta}(z_t, r, t; \tilde{y}_{\text{obs}})$.

We define a stop-gradient regression target as:

$$w_{\text{tgt}} := v - (t - r) \text{JVP}_{(z, r, t)}(w_{\theta}; (v, 0, 1)), \quad (7)$$

where, treating r as a constant,

$$\begin{aligned} & \text{JVP}_{(z, r, t)}(w_{\theta}; (v, 0, 1)) \\ &= v \partial_z w_{\theta}(z_t, r, t; \tilde{y}_{\text{obs}}) + \partial_t w_{\theta}(z_t, r, t; \tilde{y}_{\text{obs}}). \end{aligned}$$

We then minimize the mean-squared loss:

$$\mathcal{L}_{\text{EO}}(\theta) := \mathbb{E} \left[\left\| w_{\theta}(z_t, r, t; \tilde{y}_{\text{obs}}) - \text{sg}(w_{\text{tgt}}) \right\|^2 \right], \quad (8)$$

where the expectation is taken over (x, y_{obs}) , ξ , and (r, t) , and the norm is evaluated in the encoded space (the **Encode-only** setting). The resulting training and sampling procedures are summarized in Algorithms 1–2, with hyperparameters listed in Appendix E.

Encode-only vs. Encode–Decode objectives. In the *encode-only* setting we train w_{θ} by minimizing (8). Since the loss is a mean-squared regression in the encoded coordinates, its population minimizer is the conditional mean

$$w^*(z_t, r, t; \tilde{y}_{\text{obs}}) = \mathbb{E} [w_{\text{tgt}} \mid z_t, r, t, \tilde{y}_{\text{obs}}],$$

and for any θ we have the standard decomposition

$$\begin{aligned} \mathcal{L}_{\text{EO}}(\theta) &= \mathbb{E} \left[\left\| w_{\theta} - w^* \right\|^2 \right] + \mathbb{E} \left[\left\| w_{\text{tgt}} - w^* \right\|^2 \right] \\ &\geq \mathbb{E} \left[\left\| w_{\text{tgt}} - w^* \right\|^2 \right] = \mathbb{E} \left[\text{Var} (w_{\text{tgt}} \mid z_t, r, t, \tilde{y}_{\text{obs}}) \right]. \end{aligned}$$

We also consider an *Encode–Decode* variant (Algorithms 3–4), where the regression error is evaluated after decoding back to physical space. Since w_θ predicts an averaged velocity in the encoded coordinates, we map it to physical space via the Jacobian of the decoder $J(z) := D\mathcal{E}_x^{-1}(z)$, and define

$$\mathcal{L}_{\text{ED}}(\theta) := \mathbb{E} \left[\left\| J(z_t) w_\theta(z_t, r, t; \tilde{y}_{\text{obs}}) - \text{sg}(J(z_t) w_{\text{tgt}}) \right\|^2 \right]. \quad (9)$$

where the norm is taken in the physical space.

Equivalently, this loss can be viewed as a *weighted* conditional-mean regression in the encoded coordinates, with weight operator $(J(z_t))^* J(z_t)$, since

$$\|J(z_t) u\|^2 = \langle u, (J(z_t))^* J(z_t) u \rangle. \quad (10)$$

Thus, Encode-only and Encode–Decode correspond to the same conditional-mean principle, but in different geometries: Encode-only performs an unweighted CEM in the encoded space, whereas Encode–Decode performs a weighted CEM induced by the decoder. This distinction is benign for prior-aligned trace-class references, but becomes critical under a white-noise reference, where Encode–Decode *fails* empirically (see Table 3).

3.5 Theory: reference geometry and transport regularity

In this section, we justify why a prior-aligned trace-class (anisotropic) reference yields a resolution-robust geometry for one-step transport, while a discretization-level white reference is obstructed in the function-space limit. Detailed assumptions and proofs are deferred to Appendix C.

3.5.1 Trace-class reference implies Lipschitz one-step transport

We work on a separable Hilbert space \mathcal{H} . Let the reference (latent) measure be the centered trace-class Gaussian $\rho = \gamma_A = \mathcal{N}(0, C)$. Under a standard Gaussian-tail regularity condition on the posterior density in the C -geometry (Assumption C.1 in Appendix C), the mean velocity is globally Lipschitz with a dimension-free constant, which implies the existence of a globally Lipschitz one-step map.

Theorem 3.2 (Informal). *Assume the Gaussian-tail condition in Assumption C.1. The averaged velocity $w(\cdot; 0, 1)$ is globally Lipschitz on \mathcal{H} and the one-step map*

$$\mathcal{T}(\xi; y_{\text{obs}}) := \xi - w(\xi; 0, 1), \quad \xi \in \mathcal{H},$$

is globally Lipschitz with $\text{Lip}(\mathcal{T}(\cdot; y_{\text{obs}})) \leq 1 + \frac{L_0}{2}$, where L_0 depends only on the Gaussian-tail parameters.

The assumptions, statement, and proofs are provided in Appendix C.1.

3.5.2 White reference is obstructed in the function-space regime

In PDE inverse problems, the posterior $\pi(\cdot | y_{\text{obs}})$ typically lives on the same \mathcal{H} as a trace-class Gaussian prior as in (2) and is often absolutely continuous w.r.t. it. In contrast, white noise does not take values in \mathcal{H} in the mesh-refinement limit. This support mismatch manifests as mutual singularity on a distribution space \mathcal{H}^{-s} , and rules out any regular deterministic one-step transport realized as a map $\mathcal{H} \rightarrow \mathcal{H}$.

Proposition 3.3 (White vs. trace-class Gaussian are mutually singular). *Let ρ_W be the law of white noise and ρ_A the law of a trace-class Gaussian on \mathcal{H}^{-s} (definitions in Proposition C.6). Then $\rho_W \perp \rho_A$. Moreover, if $\pi \ll \rho_A$ and $\pi(\mathcal{H}) = 1$, then $\rho_W \perp \pi$.*

Proof and a concrete pushforward example are given in Appendix C.2.

4 Experiments

In this section, we evaluate the proposed one-step flow-based generative model approach on four PDE inverse problems: Darcy flow, Advection, Reaction–Diffusion, and Navier–Stokes.

4.1 PDE inverse problems and forward solvers

In this subsection, we set up the PDE inverse problems and their Bayesian solutions. Furthermore, we list the discretized numerical schemes for the forward problem used in the MCMC solver and for training data generation.

- (1) Darcy flow. We infer the positive permeability $a : \Omega \rightarrow \mathbb{R}^+$ on $\Omega = [0, 1]^2$ from noisy observations of the hydraulic head u satisfying the steady Darcy equation

$$\begin{cases} -\nabla \cdot (a \nabla u) = f & \text{in } \Omega, \\ u = 0 & \text{on } \partial\Omega. \end{cases} \quad (11)$$

with forward map $\mathcal{G}(\log a) = u$. To enforce positivity, we place a Gaussian prior on $\log a$: $\log a \sim \mathcal{N}(0, (-\Delta + 9I)^{-2})$. We discretize (11) by a finite-volume TPFA scheme, yielding a sparse SPD linear system (Appendix B.1). The experiments use a 65×65 grid. Observations follow $y_{\text{obs}} = \mathcal{O}_{\text{int}}(u) + \eta$ where $\eta \sim \mathcal{N}(0, I_m)$. \mathcal{O}_{int} denotes an interior equidistant subsampling operator that avoids boundary points, producing 7×7 measurements ($m = 49$).

In the following fluid equations (Advection, RDE, NSE), we consider a periodic domain $\Omega = [0, 1)^2$ and time variable $\tau > 0$. All experiments use a 64×64 grid. The observation operator \mathcal{O}_{per} uniformly subsamples the full periodic grid (without removing boundary points) at 8×8 locations ($m = 64$). The standard deviation of the observation noise η is chosen to be adapted to the output function value, specified individually.

- (2) Advection. In the 2D linear Advection equation,

$$\begin{cases} \partial_\tau u + \mathbf{b} \cdot \nabla u = 0 & \text{in } \Omega \times (0, \infty), \\ u(\cdot, 0) = u_0 & \text{in } \Omega, \end{cases} \quad (12)$$

with velocity $\mathbf{b} = (b_1, b_2)$, we consider the forward map $\mathcal{G}(u_0) = u(\cdot, T = 1)$. On the computational grid, we discretize (12) using a first-order upwinding in space and forward Euler in time scheme under a CFL constraint (Appendix B.2). The observations are $y_{\text{obs}} = \mathcal{O}_{\text{per}}(u) + \eta$ with $\eta \sim \mathcal{N}(0, 0.05^2 I_m)$.

- (3) Reaction–Diffusion Equation (RDE). The 2D Allen–Cahn Reaction–Diffusion equation follows:

$$\begin{cases} \partial_\tau u = D \Delta u + u - u^3 & \text{in } \Omega \times (0, \infty), \\ u(\cdot, 0) = u_0 & \text{in } \Omega, \end{cases} \quad (13)$$

with diffusion coefficient $D > 0$. We consider the forward map $\mathcal{G}(u_0) = u(\cdot, T = 2)$. We discretize (13) on a uniform grid using the standard second-order central-difference Laplacian and forward Euler time stepping (Appendix B.3). Observations follow $y_{\text{obs}} = \mathcal{O}_{\text{per}}(u) + \eta$ where $\eta \sim \mathcal{N}(0, 0.05^2 I_m)$.

- (4) Navier–Stokes Equation (in vorticity form, NSE). In the 2D vorticity formulation

$$\begin{cases} \partial_\tau u + \mathbf{q} \cdot \nabla u = \nu \Delta u + g, & \text{in } \Omega \times (0, \infty), \\ -\Delta \psi = u, & \text{in } \Omega, \\ \mathbf{q} = \nabla^\perp \psi := (\partial_2 \psi, -\partial_1 \psi), & \text{in } \Omega, \\ u(\cdot, 0) = u_0, & \text{in } \Omega, \end{cases} \quad (14)$$

where $\nu > 0$ is the viscosity and g is a fixed forcing. we consider the forward map $\mathcal{G}(u_0) = u(\cdot, T = 0.2)$. We solve (14) using a Fourier pseudo-spectral method with 2/3 de-aliasing and an IMEX time integrator (Crank-Nicolson for diffusion and explicit advection); see Appendix B.4 for details. Observations follow $y_{\text{obs}} = \mathcal{O}_{\text{per}}(u) + \eta$ where $\eta \sim \mathcal{N}(0, 0.01^2 I_m)$.

4.2 Posterior statistics and error metrics

We assess posterior quality via the posterior mean and standard deviation. For any test observation y_{obs} , our model induces an approximate posterior distribution by varying only the latent/reference draw. Specifically, we sample $\xi^{(i)} \sim \rho$ i.i.d. and generate $N_{\text{eval}} = 10^3$ posterior samples $x_{\text{pred}}^{(i)} = \mathcal{T}_{\hat{\theta}}(\xi^{(i)}; y_{\text{obs}})$ for the same y_{obs} on the spatial grids. We then estimate the posterior mean field μ_{pred} and the (pointwise) standard deviation field σ_{pred} :

$$\mu_{\text{pred}} = \frac{1}{N_{\text{eval}}} \sum_{i=1}^{N_{\text{eval}}} x_{\text{pred}}^{(i)},$$

$$\sigma_{\text{pred}} = \sqrt{\frac{1}{N_{\text{eval}} - 1} \sum_{i=1}^{N_{\text{eval}}} (x_{\text{pred}}^{(i)} - \mu_{\text{pred}})^2},$$

where operations are taken pointwise over the spatial grid.

As reference, we use ground-truth posterior statistics μ_{true} and σ_{true} , computed from trustworthy MCMC samples $\{x_{\text{ref}}^{(i)}\}_{i=1}^{N_{\text{MCMC}}}$ for PDE inverse problems with $N_{\text{MCMC}} = 10^3$ for fair comparison.

The construction and validation of the reference posterior statistics are detailed in Appendix A.2. Although accurate, MCMC is not amortized: each new observation y_{obs} requires running a fresh Markov chain. By contrast, once trained, our conditional model can be reused for arbitrary y_{obs} . Moreover, obtaining reliable MCMC statistics is computationally expensive (Table 1). These limitations motivate our one-step sampler design.

Remark 4.1 (Fair comparison and KL dimension). For all methods we fix the KL truncation to $N_{\text{KL}} = 64$ in PDE inverse problems to enable a fair and tractable comparison. In coefficient space, increasing N_{KL} typically worsens MCMC mixing and inflates the integrated autocorrelation time, making reliable posterior statistics prohibitively expensive. We note that a smaller N_{KL} may also *simplify* the inference task (in particular, with white-noise as reference distribution ρ) by removing high-frequency degrees of freedom. Importantly, the time cost of our one-step sampler is essentially independent of the KL dimension: even with the full basis ($N^2 - 1$ modes), sampling still requires only a single network forward pass (no iterative Markov steps).

We quantify discrepancies using relative L^2 errors for both mean and uncertainty:

$$\epsilon_{\mu}^{\text{eval}} = \|\mu_{\text{pred}} - \mu_{\text{true}}\|_{L^2(\Omega)} / \|\mu_{\text{true}}\|_{L^2(\Omega)},$$

$$\epsilon_{\sigma}^{\text{eval}} = \|\sigma_{\text{pred}} - \sigma_{\text{true}}\|_{L^2(\Omega)} / \|\sigma_{\text{true}}\|_{L^2(\Omega)}.$$

Figures 3–6 summarize the Encode-only model results for each PDE inverse problem under the prior-aligned anisotropic reference. In each figure, the first row visualizes the ground-truth unknown (coefficient or initial condition), the associated PDE solution, and the observations (before adding noise). The second row shows the learned and reference posterior means and their difference. Table 2 reports the results for both reference choices.

Overall, under our experimental setup with a prior-aligned anisotropic reference, we achieve $\epsilon_{\mu}^{\text{eval}} < 10\%$ and $\epsilon_{\sigma}^{\text{eval}} < 10\%$ across all PDE inverse problems considered (Darcy, Advection, Reaction–Diffusion, and Navier–Stokes), indicating accurate recovery of both the posterior mean and posterior uncertainty relative to the reference posterior. With the white-reference, $\epsilon_{\mu}^{\text{eval}}$ and $\epsilon_{\sigma}^{\text{eval}}$ remain close to those of the anisotropic-reference baseline at the tested resolutions because

Table 1: Wall-clock generation time for producing posterior samples *conditioned on a single fixed observation* y_{obs} . *Hardware*: MCMC is run in parallel on 16 cores of the CPU (32 thread at 3.6GHz) cores; learned samplers are evaluated on a single NVIDIA RTX A6000 GPU. The per-sample clock time is computed by averaging over the generation time of 1000 posterior samples.

Sampler	Steps	Time / sample (s)
MCMC (Darcy)	3×10^4	2.05×10^1
MCMC (Advection)	3×10^4	7.01
MCMC (Reaction–Diffusion)	3×10^4	1.04×10^1
MCMC (Navier–Stokes)	3×10^4	1.97×10^1
Multistep Diffusion	320	1.05×10^{-1}
One-step (MF)	1	3.50×10^{-4}
One-step (iMF)	1	3.51×10^{-4}
One-step (PODNO backbone)	1	3.17×10^{-4}
One-step (U-Net backbone)	1	1.85×10^{-3}

Note: Generation of training data (10000) requires 432s for Darcy, 75s for Advection, 145s for Reaction–Diffusion, 385s for Navier–Stokes.

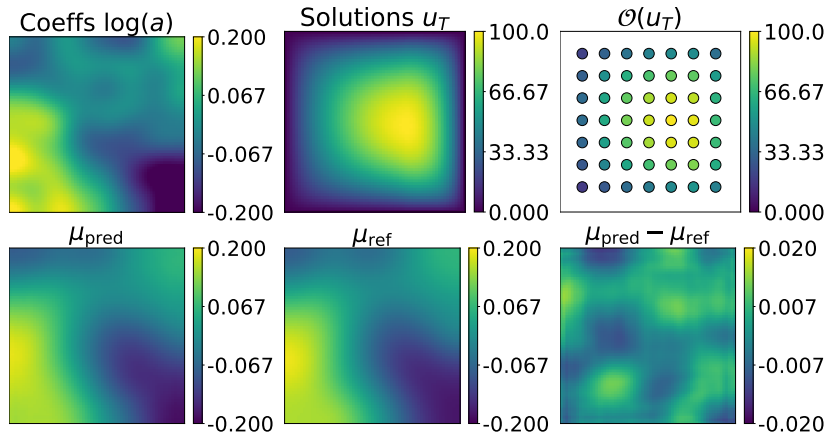


Figure 3: **Darcy Equation**. 3×3 visualization: (Top) ground truth and observations, (Bottom) posterior means. Reference: $\rho_A = \mathcal{N}(0, (-\Delta_{\text{Neumann}} + 9I)^{-2})$. Noise level: $\sigma_\eta = 1$.

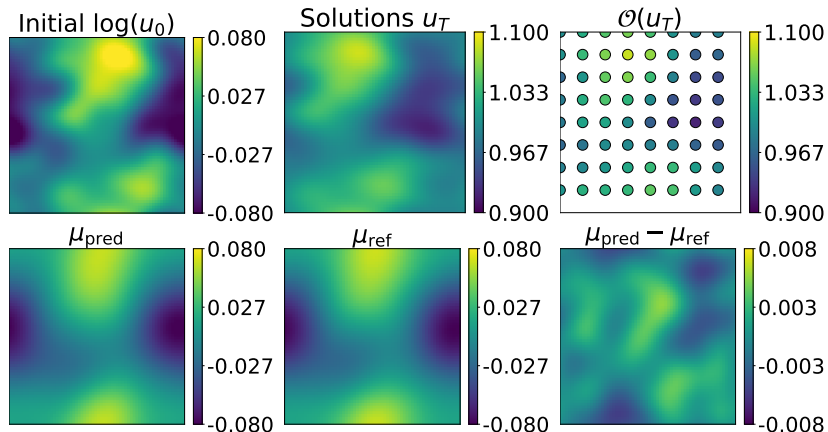


Figure 4: **Advection Equation**. 3×3 visualization: (Top) ground truth and observations, (Bottom) posterior means. Reference: $\rho_A = \mathcal{N}(0, (-\Delta_{\text{per}} + 9I)^{-2})$. Noise level: $\sigma_\eta = 0.05$.

unit-Gaussian normalization and the KL truncation $N_{\text{KL}} = 64$ in the MCMC reference generator suppress high-frequency mismatch found in Figure 1.

Despite such preconditioning (unit-Gaussian normalization) may yield a marginal improvement in terms of ϵ_σ in some realization of tests, such discretization dependent mechanism is

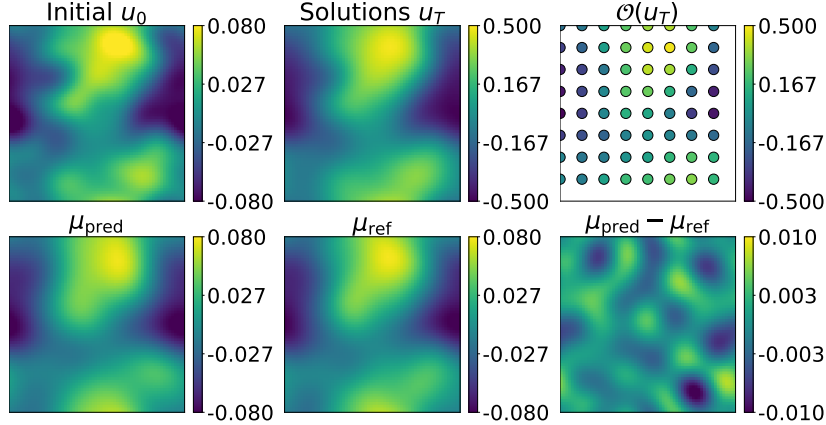


Figure 5: **Reaction-Diffusion Equation.** 3×3 visualization: (Top) ground truth and observations, (Bottom) posterior means. Reference: $\rho_A = \mathcal{N}(0, (-\Delta_{\text{per}} + 9I)^{-2})$. Noise level: $\sigma_\eta = 0.05$.

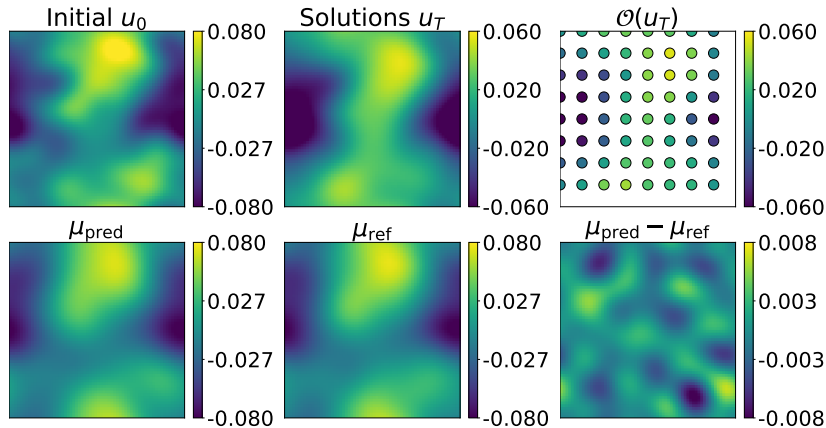


Figure 6: **Navier-Stokes Equation.** 3×3 visualization: (Top) ground truth and observations, (Bottom) posterior means. Reference: $\rho_A = \mathcal{N}(0, (-\Delta_{\text{per}} + 9I)^{-2})$. Noise level: $\sigma_\eta = 0.01$.

Table 2: Evaluation results across different inverse problems and reference types, using an Encode-only Mean Flows model with an FNO backbone.

Dataset	Reference	$\epsilon_\mu^{\text{eval}}$	$\epsilon_\sigma^{\text{eval}}$
Darcy	Anisotropic	5.55×10^{-2}	4.27×10^{-2}
	White	8.26×10^{-2}	4.30×10^{-2}
Advection	Anisotropic	6.08×10^{-2}	5.09×10^{-2}
	White	1.63×10^{-1}	5.14×10^{-2}
Reaction-Diffusion	Anisotropic	7.62×10^{-2}	8.68×10^{-2}
	White	7.89×10^{-2}	8.91×10^{-2}
Navier-Stokes	Anisotropic	6.41×10^{-2}	5.39×10^{-2}
	White	8.16×10^{-2}	5.26×10^{-2}

Note: The singularity between the white reference and the anisotropic posterior is mitigated by our Encode-only setting, but it re-emerges in the Encode-Decode model and in the improved Mean Flows variants as shown in Appendix D.

fragile: the gap between the summary metrics $\epsilon_\mu^{\text{eval}}$ and $\epsilon_\sigma^{\text{eval}}$ and the underlying sample quality becomes much more pronounced when learning is performed in physical space (the Encode-Decode variant), where high-frequency mismatches are penalized more strongly (see Table 3). Moreover, under the improved Mean Flows objective, the white-noise reference exhibits severe numerical instability and can diverge even when training is carried out in the encoded space, whereas the prior-aligned anisotropic reference remains stable (see Table 6). Taken together, these results suggest that the mild white-reference performance observed for the Encode-only

model at finite resolution is not fundamental.

Additional *ablations* with alternative operator-learning backbones (PODNO; Table 4) and a finite-dimensional U-Net learning backbone (Table 5), together with a multistep diffusion model for comparison (Table 7), are reported in Appendix D and reinforce two key takeaways. First, performance is largely backbone-agnostic *within operator-learning architectures*, underscoring the necessity of an infinite-dimensional (resolution-robust) design. Second, compared with multistep diffusion, our one-step generative transport yields faster sampling and more accurate posterior summaries under the observation setting considered.

5 Conclusive remarks and limitations

We develop an amortized, observation-conditional one-step model: once trained, it generates posterior samples for any new y_{obs} without retraining, and does so in a single forward pass—substantially faster than multistep diffusion and MCMC. Training is purely data-driven from forward solver of priors, with no teacher model or MCMC supervision. We prove that the reference-measure choice is decisive in function space: transports are well-posed under trace-class references but can be intrinsically ill-posed under white-noise references due to measure singularity; experiments confirm this and an Encode-only heuristic partially mitigates white-noise baselines at finite resolution.

Limitations. Overall performance depends on the expressivity and conditioning of the operator backbone; current neural operators may struggle with highly anisotropic or multiscale posteriors. Moreover, we currently lack principled diagnostics for the approximation error of the learned velocity, making bias in uncertainty estimates hard to detect. Finally, training requires offline PDE simulations, incurring additional computational and storage costs.

Impact statement

This paper studies machine-learning methods for PDE-based inverse problems in scientific computing. While such methods may impact a broad range of downstream applications, we do not foresee immediate societal risks that require specific discussion beyond standard considerations on data, robustness, and responsible deployment.

Acknowledgements

This work was supported by Singapore MOE AcRF Tier 1 Grant RG95/23 and RG17/24, NTU SUG-023162-00001, and Singapore MOE AcRF Tier 2 Grant: MOE-T2EP20224-0012.

References

- [1] Michael Samuel Albergo and Eric Vanden-Eijnden. Building normalizing flows with stochastic interpolants. In *The Eleventh International Conference on Learning Representations*, 2023.
- [2] James L Beck and Lambros S Katafygiotis. Updating models and their uncertainties. I: Bayesian statistical framework. *Journal of Engineering Mechanics*, 124(4):455–461, 1998.
- [3] Gabriel Cardoso, Yazid Janati el idrissi, Sylvain Le Corff, and Eric Moulines. Monte Carlo guided denoising diffusion models for Bayesian linear inverse problems. In *The Twelfth International Conference on Learning Representations*, 2024.

- [4] Zilan Cheng, Zhongjian Wang, Li-Lian Wang, and Mejdi Azaiez. PODNO: Proper orthogonal decomposition neural operators. *arXiv preprint arXiv:2504.18513*, 2025.
- [5] Simon L Cotter, Gareth O Roberts, Andrew M Stuart, and David White. MCMC methods for functions: modifying old algorithms to make them faster. *Statistical Science*, pages 424–446, 2013.
- [6] Masoumeh Dashti and Andrew M Stuart. The Bayesian approach to inverse problems. In *Handbook of uncertainty quantification*, pages 1–118. Springer, 2015.
- [7] Prafulla Dhariwal and Alexander Quinn Nichol. Diffusion models beat GANs on image synthesis. In A. Beygelzimer, Y. Dauphin, P. Liang, and J. Wortman Vaughan, editors, *Advances in Neural Information Processing Systems*, 2021.
- [8] Zehao Dou and Yang Song. Diffusion posterior sampling for linear inverse problem solving: A filtering perspective. In *The Twelfth International Conference on Learning Representations*, 2024.
- [9] Zhengyang Geng, Mingyang Deng, Xingjian Bai, J Zico Kolter, and Kaiming He. Mean Flows for one-step generative modeling. In *The Thirty-ninth Annual Conference on Neural Information Processing Systems*, 2025.
- [10] Zhengyang Geng, Yiyang Lu, Zongze Wu, Eli Shechtman, J Zico Kolter, and Kaiming He. Improved Mean Flows: On the challenges of fastforward generative models. *arXiv preprint arXiv:2512.02012*, 2025.
- [11] Jonathan Goodman and Jonathan Weare. Ensemble samplers with affine invariance. *Communications in applied mathematics and computational science*, 5(1):65–80, 2010.
- [12] Jonathan Ho, Ajay Jain, and Pieter Abbeel. Denoising diffusion probabilistic models. In H. Larochelle, M. Ranzato, R. Hadsell, M.F. Balcan, and H. Lin, editors, *Advances in Neural Information Processing Systems*, volume 33, pages 6840–6851. Curran Associates, Inc., 2020.
- [13] Jiahe Huang, Guandao Yang, Zichen Wang, and Jeong Joon Park. DiffusionPDE: Generative PDE-solving under partial observation. In *The Thirty-eighth Annual Conference on Neural Information Processing Systems*, 2024.
- [14] Marco A Iglesias, Kui Lin, and Andrew M Stuart. Well-posed Bayesian geometric inverse problems arising in subsurface flow. *Inverse problems*, 30(11):114001, 2014.
- [15] Marc C Kennedy and Anthony O’Hagan. Bayesian calibration of computer models. *Journal of the Royal Statistical Society: Series B (Statistical Methodology)*, 63(3):425–464, 2001.
- [16] Zongyi Li, Nikola Borislavov Kovachki, Kamyar Azizzadenesheli, Burigede Liu, Kaushik Bhattacharya, Andrew Stuart, and Anima Anandkumar. Fourier neural operator for parametric partial differential equations. In *International Conference on Learning Representations*, 2021.
- [17] Jae Hyun Lim, Nikola B Kovachki, Ricardo Baptista, Christopher Beckham, Kamyar Azizzadenesheli, Jean Kossaiji, Vikram Voleti, Jiaming Song, Karsten Kreis, Jan Kautz, et al. Score-based diffusion models in function space. *Journal of Machine Learning Research*, 26(158):1–62, 2025.
- [18] Yaron Lipman, Ricky T. Q. Chen, Heli Ben-Hamu, Maximilian Nickel, and Matthew Le. Flow matching for generative modeling. In *The Eleventh International Conference on Learning Representations*, 2023.

- [19] Xingchao Liu, Chengyue Gong, and Qiang Liu. Flow straight and fast: Learning to generate and transfer data with rectified flow. In *The Eleventh International Conference on Learning Representations*, 2023.
- [20] Ziyuan Liu, Haifeng Wang, Hong Zhang, Kaijun Bao, Xu Qian, and Songhe Song. Render unto numerics: Orthogonal polynomial neural operator for PDEs with nonperiodic boundary conditions. *SIAM Journal on Scientific Computing*, 46(4):C323–C348, 2024.
- [21] Lu Lu, Pengzhan Jin, Guofei Pang, Zhongqiang Zhang, and George Em Karniadakis. Learning nonlinear operators via DeepONet based on the universal approximation theorem of operators. *Nature Machine Intelligence*, 3(3):218–229, 2021.
- [22] Alberto Malinverno. Parsimonious Bayesian Markov chain Monte Carlo inversion in a nonlinear geophysical problem. *Geophysical Journal International*, 151(3):675–688, 2002.
- [23] Xiangjun Meng and Zhongjian Wang. Pathway to $o(\sqrt{d})$ complexity bound under Wasserstein metric of flow-based models. *arXiv preprint arXiv:2512.06702*, 2025.
- [24] Aliaksandra Shysheya, Cristiana Diaconu, Federico Bergamin, Paris Perdikaris, José Miguel Hernández-Lobato, Richard E. Turner, and Emile Mathieu. On conditional diffusion models for PDE simulations. In *The Thirty-eighth Annual Conference on Neural Information Processing Systems*, 2024.
- [25] Yang Song, Liyue Shen, Lei Xing, and Stefano Ermon. Solving inverse problems in medical imaging with score-based generative models. In *International Conference on Learning Representations*, 2022.
- [26] Yang Song, Jascha Sohl-Dickstein, Diederik P Kingma, Abhishek Kumar, Stefano Ermon, and Ben Poole. Score-based generative modeling through stochastic differential equations. In *International Conference on Learning Representations*, 2021.
- [27] Andrew M Stuart. Inverse problems: a Bayesian perspective. *Acta numerica*, 19:451–559, 2010.
- [28] Yasi Zhang, Peiyu Yu, Yaxuan Zhu, Yingshan Chang, Feng Gao, Ying Nian Wu, and Oscar Leong. Flow priors for linear inverse problems via iterative corrupted trajectory matching. *Advances in Neural Information Processing Systems*, 37:57389–57417, 2024.
- [29] Qingping Zhou, Tengchao Yu, Xiaoqun Zhang, and Jinglai Li. Bayesian inference and uncertainty quantification for medical image reconstruction with Poisson data. *SIAM Journal on Imaging Sciences*, 13(1):29–52, 2020.

A Ground-truth Posterior Generation and Validation

In this appendix, we describe how the ground-truth posterior distributions used throughout the experiments are constructed, and why they can be regarded as trustworthy references for evaluating the proposed Bayesian inverse problems operator models. Two different strategies are employed, depending on the inverse problem.

A.1 Identity Map: Closed-form Posterior

Problem setting. We consider the identity forward map $\mathcal{G}(x) = x$ on $\Omega = [0, 1]^2$ and noisy partial observations

$$y_{\text{obs}} = \mathcal{O}(x) + \eta, \quad \eta \sim \mathcal{N}(0, \sigma_\eta^2 I_m),$$

where \mathcal{O} is a linear subsampling operator selecting m spatial locations randomly, $\sigma_\eta = 0.1$. After discretization on an $N \times N$ -point grid, we identify $x \in \mathbb{R}^{N^2}$ with its grid values and write

$$y_{\text{obs}} = Hx + \eta, \quad \eta \sim \mathcal{N}(0, \sigma_\eta^2 I_m),$$

where $H \in \mathbb{R}^{m \times N^2}$ is the corresponding (random) selection matrix.

Prior (trace-class GRF) and RKHS geometry. We impose a zero-mean Gaussian random field prior

$$x \sim \mathcal{N}(0, C), \quad C = (\kappa^2 I - \Delta_{\text{Neumann}})^{-d},$$

where Δ_{Neumann} is the Neumann Laplacian on Ω , $\kappa > 0$ sets a correlation length, and $d > 1$ ensures that C is trace-class on $L^2(\Omega)$. We set $\kappa = 3$ and $d = 2$. With the cosine eigenbasis $\{e_k\}_{k \in \mathbb{N}_0^2}$ of $-\Delta_{\text{Neumann}}$,

$$-\Delta_{\text{Neumann}} e_k = \pi^2 |k|^2 e_k, \quad |k|^2 = k_1^2 + k_2^2,$$

the covariance is diagonal and has eigenvalues

$$\lambda_k = (\pi^2 |k|^2 + \kappa^2)^{-d}.$$

A prior draw admits the KL expansion

$$x(\cdot) = \sum_{k \in \mathbb{N}_0^2} \sqrt{\lambda_k} h_k e_k, \quad h_k \stackrel{\text{i.i.d.}}{\sim} \mathcal{N}(0, 1),$$

and we denote by $x = \Psi(h) \in \mathbb{R}^{N^2}$ the corresponding discretized field on the $N \times N$ grid

Remark A.1 (Choice of KL truncation). For the identity model, the posterior is Gaussian and available in closed form. For PDE inverse problems, we approximate the posterior via MCMC and, for computational tractability, typically truncate the KL expansion (e.g., to 64 modes).

The associated Cameron–Martin/RKHS norm can be expressed in the eigenbasis as

$$\|x\|_{\mathcal{H}}^2 = \sum_{k \in \mathbb{N}_0^2} \frac{|x_k|^2}{\lambda_k}, \quad x_k := \langle x(\cdot), e_k \rangle_{L^2(\Omega)}.$$

Closed-form posterior distribution. In the discretized setting, since x and η are independent Gaussians and $y_{\text{obs}} = Hx + \eta$ is linear in (x, η) , the joint vector (x, y_{obs}) is Gaussian:

$$\begin{pmatrix} x \\ y_{\text{obs}} \end{pmatrix} \sim \mathcal{N} \left(\begin{pmatrix} 0 \\ 0 \end{pmatrix}, \begin{pmatrix} C & CH^\top \\ HC & HCH^\top + \sigma_\eta^2 I_m \end{pmatrix} \right).$$

By the conditional Gaussian formula,

$$x \mid y_{\text{obs}} \sim \mathcal{N}(\mu_{x|y_{\text{obs}}}, \Sigma_{x|y_{\text{obs}}}),$$

where

$$\mu_{x|y_{\text{obs}}} = CH^\top (HCH^\top + \sigma_\eta^2 I_m)^{-1} y_{\text{obs}}, \quad \Sigma_{x|y_{\text{obs}}} = C - CH^\top (HCH^\top + \sigma_\eta^2 I_m)^{-1} HC.$$

Thus, in the discretized setting we take the ground-truth posterior mean and pointwise standard deviation as:

$$\mu_{\text{true}} := \mu_{x|y_{\text{obs}}}, \quad \sigma_{\text{true}} := \sqrt{\text{diag}(\Sigma_{x|y_{\text{obs}}})}.$$

Remark A.2 (Variational interpretation and MAP). The likelihood induced by $y_{\text{obs}} = Hx + \eta$ with $\eta \sim \mathcal{N}(0, \sigma_\eta^2 I_m)$ is

$$p(y_{\text{obs}} \mid x) \propto \exp \left(-\frac{1}{2\sigma_\eta^2} \|Hx - y_{\text{obs}}\|_2^2 \right),$$

and the (discretized) Gaussian prior $x \sim \mathcal{N}(0, C)$ satisfies

$$p(x) \propto \exp \left(-\frac{1}{2} x^\top C^{-1} x \right).$$

Hence, $p(x \mid y_{\text{obs}}) \propto p(y_{\text{obs}} \mid x)p(x)$ and the MAP estimator minimizes the negative log-posterior (up to an additive constant):

$$x_{\text{MAP}} = \arg \min_{x \in \mathcal{H}} \left(\frac{1}{2} x^\top C^{-1} x + \frac{1}{2\sigma_\eta^2} \|Hx - y_{\text{obs}}\|_2^2 \right) = \arg \min_{x \in \mathcal{H}} \left(\frac{1}{2} \|x\|_{\mathcal{H}}^2 + \frac{1}{2\sigma_\eta^2} \|Hx - y_{\text{obs}}\|_2^2 \right),$$

where $\|x\|_{\mathcal{H}}^2 := x^\top C^{-1} x$ is the Cameron–Martin (RKHS) norm. The first-order optimality condition reads

$$(C^{-1} + \sigma_\eta^{-2} H^\top H)x = \sigma_\eta^{-2} H^\top y_{\text{obs}},$$

and the Woodbury identity yields $x_{\text{MAP}} = CH^\top (HCH^\top + \sigma_\eta^2 I_m)^{-1} y_{\text{obs}} = \mu_{x|y_{\text{obs}}}$.

In this linear-Gaussian identity problem, both the posterior mean and covariance are available in closed form, with no other error. We therefore use this setting as a ground-truth benchmark for posterior learning and uncertainty quantification.

A.2 PDE Inverse Problems: MCMC Reference Posterior

Problem setting. For the PDE-based inverse problems (Darcy flow, advection, reaction-diffusion, and Navier-Stokes), the forward operator \mathcal{G} is nonlinear and is defined implicitly through a PDE solver. We assume additive Gaussian observation noise and consider the observation model

$$y_{\text{obs}} = \mathcal{O}(\mathcal{G}(x)) + \eta, \quad \eta \sim \mathcal{N}(0, \sigma_\eta^2 I_m),$$

where x denotes the unknown field (e.g., log-permeability, an initial condition, etc.) and \mathcal{O} is the observation operator. Writing the prior as γ , Bayes' rule yields the posterior

$$\pi(dx \mid y_{\text{obs}}) \propto \exp \left(-\frac{1}{2\sigma_\eta^2} \|\mathcal{O}(\mathcal{G}(x)) - y_{\text{obs}}\|_2^2 \right) \gamma(dx),$$

which is generally non-Gaussian and does not admit a closed-form expression.

Prior. We employ Gaussian random field (GRF) priors consistent with the boundary conditions of each PDE.

(i) *Darcy flow (non-periodic boundary).* For Darcy, we use the same Neumann GRF prior as in the identity benchmark:

$$x \sim \mathcal{N}(0, C), \quad C = (\kappa^2 I - \Delta_{\text{Neumann}})^{-d},$$

where Δ_{Neumann} is the Neumann Laplacian on $\Omega = [0, 1]^2$. For MCMC, we work with a truncated Karhunen-Loève (KL) expansion and retain the leading 64 modes of C .

(ii) *Advection, reaction-diffusion, and Navier–Stokes (periodic boundary).* On periodic domains, we adopt a GRF prior diagonalized by Fourier modes. Let $k = (k_1, k_2) \in \mathbb{Z}^2$ be the wavevector. The covariance is specified via the spectral density

$$\lambda_k = \left((2\pi)^2 |k|^2 + \kappa^2 \right)^{-d},$$

and we represent the field using real Fourier pairs $\cos(2\pi k \cdot x)$ and $\sin(2\pi k \cdot x)$. In practice, we truncate to $N_{\text{KL}} = 64$ KL coefficients (real Fourier basis), ordered by increasing $|k|^2$. We set $\kappa = 3$ and $d = 2$; in 2D, $d > 1$ ensures that the resulting covariance operator is trace-class on $L^2(\Omega)$.

MCMC reference posterior (coefficient-space MCMC). We sample from the posterior over truncated KL coefficients and map these samples to the field space via the KL synthesis map. Let $h = (h_1, \dots, h_{N_{\text{KL}}}) \in \mathbb{R}^{N_{\text{KL}}}$ denote the truncated KL coefficients and let $x = \Psi(h) \in \mathbb{R}^{N^2}$ be the corresponding field reconstructed by the truncated KL synthesis map. Under the KL parameterization, the prior becomes standard Gaussian,

$$h \sim \mathcal{N}(0, I_{N_{\text{KL}}}),$$

and the posterior on coefficients is

$$\pi(h \mid y_{\text{obs}}) \propto \exp\left(-\frac{1}{2\sigma_\eta^2} \|\mathcal{O}(\mathcal{G}(\Psi(h))) - y_{\text{obs}}\|_2^2\right) \exp\left(-\frac{1}{2} \|h\|_2^2\right).$$

We draw samples from $\pi(h \mid y_{\text{obs}})$ using the affine-invariant ensemble sampler implemented in `emcee` [11]. Each coefficient sample $h^{(i)}$ is mapped to a field sample $x_{\text{ref}}^{(i)} := \Psi(h^{(i)})$ to form the reference posterior sample set in function space.

For practicality, we run MCMC in a truncated KL coefficient space with $N_{\text{KL}} = 64$. Larger KL dimensions substantially worsen mixing and typically inflate the integrated autocorrelation time, making stable posterior statistics prohibitively expensive in our PDE inverse problems; even with $N_{\text{KL}} = 64$, the wall-clock cost is already substantial (Table 1). Given this parameter dimension, we use 200 walkers in `emcee`.

Remark A.3 (Chain length and stability criterion). We choose the MCMC chain length using the integrated autocorrelation time τ_{int} (IACT) as a practical stability criterion. Following the common heuristic that stable Monte Carlo estimates require $\mathcal{O}(50 \tau_{\text{int}})$ *post burn-in* steps, we discard the first 5,000 steps as burn-in and estimate τ_{int} from the remaining coefficient chain. Across all datasets considered here, we observe $\tau_{\text{int}} \approx 500$, so we run in total

$$N_{\text{steps}} = N_{\text{burnin}} + 50 \tau_{\text{int}} \approx 5,000 + 50 \times 500 \approx 3 \times 10^4$$

steps per chain.

From the post burn-in coefficient samples $\{h^{(i)}\}_{i=1}^{N_{\text{MCMC}}}$ where $N_{\text{MCMC}} = 10^3$, we form $x_{\text{ref}}^{(i)} = \Psi(h^{(i)})$ and compute the reference posterior statistics:

$$\mu_{\text{true}} = \frac{1}{N_{\text{MCMC}}} \sum_{i=1}^{N_{\text{MCMC}}} x_{\text{ref}}^{(i)}, \quad \sigma_{\text{true}} = \left(\frac{1}{N_{\text{MCMC}} - 1} \sum_{i=1}^{N_{\text{MCMC}}} (x_{\text{ref}}^{(i)} - \mu_{\text{true}})^2 \right)^{1/2}.$$

These empirical μ_{true} and σ_{true} are used as the trustworthy references for computing relative L^2 error of posterior mean $\epsilon_{\mu}^{\text{eval}}$ and standard deviation $\epsilon_{\sigma}^{\text{eval}}$ in the main text.

B Datasets

B.1 Darcy Flow

Model. We consider the steady Darcy equation on $\Omega = [0, 1]^2$:

$$\begin{cases} -\nabla \cdot (a \nabla u) = f, & \text{in } \Omega, \\ u = 0, & \text{on } \partial\Omega, \end{cases}$$

where u is the hydraulic head, $a > 0$ is the permeability (hydraulic conductivity), and f is a prescribed source term.

Discretization. We introduce a uniform $N \times N$ grid and denote the grid spacing by $\Delta = \frac{1}{N-1}$. Dirichlet boundary values are imposed on all boundary indices, and the unknowns are the interior values $\{u_{i,j}\}$ with $i, j = 1, \dots, N-2$.

Let $a_{i,j}$ denote the cell-centered permeability on the grid. Face permeabilities are approximated by arithmetic averages:

$$\begin{aligned} a_{i+\frac{1}{2},j} &= \frac{1}{2} (a_{i,j} + a_{i+1,j}), & a_{i-\frac{1}{2},j} &= \frac{1}{2} (a_{i,j} + a_{i-1,j}), \\ a_{i,j+\frac{1}{2}} &= \frac{1}{2} (a_{i,j} + a_{i,j+1}), & a_{i,j-\frac{1}{2}} &= \frac{1}{2} (a_{i,j} + a_{i,j-1}). \end{aligned}$$

Applying the two-point flux approximation (TPFA), the discrete equation at each interior index (i, j) is

$$\frac{1}{\Delta^2} \left[a_{i+\frac{1}{2},j} (u_{i+1,j} - u_{i,j}) - a_{i-\frac{1}{2},j} (u_{i,j} - u_{i-1,j}) + a_{i,j+\frac{1}{2}} (u_{i,j+1} - u_{i,j}) - a_{i,j-\frac{1}{2}} (u_{i,j} - u_{i,j-1}) \right] = f_{i,j}.$$

For indices adjacent to the boundary, the exterior neighbor is replaced by the Dirichlet value $u = 0$, contributing only to the diagonal coefficient.

Experiment settings. To enforce the physical constraint $a > 0$, we parameterize the permeability as a log-normal random field $a = \exp(\ell)$, where ℓ is sampled from the non-periodic (Neumann) GRF prior (truncated to $N_{\text{KL}} = 64$) described in Section A.2. The source term is piecewise constant in the second coordinate; on the grid we set $f_{i,j} = f_j$ with

$$f_j = \begin{cases} 1000, & 0 \leq j\Delta \leq \frac{4}{6}, \\ 2000, & \frac{4}{6} < j\Delta \leq \frac{5}{6}, \\ 3000, & \frac{5}{6} < j\Delta \leq 1. \end{cases}$$

B.2 Advection

Model. We consider the 2D linear advection equation on the periodic domain $\Omega = [0, 1]^2$:

$$\begin{cases} \partial_\tau u + \mathbf{b} \cdot \nabla u = 0, & \text{in } \Omega \times (0, \infty), \\ u(\cdot, 0) = u_0, & \text{in } \Omega, \end{cases}$$

where $\mathbf{b} = (b_1, b_2) \in \mathbb{R}^2$ is velocity and periodic boundary conditions are imposed.

Discretization. We use a uniform periodic $N \times N$ grid with spacings $\Delta_1 = \Delta_2 = \frac{1}{N}$, and denote the numerical solution by $u_{i,j}^n \approx u(\cdot, \tau^n)$ at time $\tau^n = n\Delta\tau$, with indices $i, j = 0, \dots, N-1$. We approximate spatial derivatives by first-order upwind differences. Let

$$b_1^+ = \max(b_1, 0), \quad b_1^- = \min(b_1, 0), \quad b_2^+ = \max(b_2, 0), \quad b_2^- = \min(b_2, 0).$$

The forward Euler upwind update is

$$u_{i,j}^{n+1} = u_{i,j}^n - \Delta\tau \left[\frac{b_1^+(u_{i,j}^n - u_{i-1,j}^n)}{\Delta_1} + \frac{b_1^-(u_{i+1,j}^n - u_{i,j}^n)}{\Delta_1} + \frac{b_2^+(u_{i,j}^n - u_{i,j-1}^n)}{\Delta_2} + \frac{b_2^-(u_{i,j+1}^n - u_{i,j}^n)}{\Delta_2} \right],$$

where periodic boundary conditions are enforced by wrapping indices, e.g. $u_{-1,j}^n = u_{N-1,j}^n$ and $u_{N,j}^n = u_{0,j}^n$ (and similarly in the second index).

Stability (CFL condition). The explicit scheme (B.2) is stable if the Courant numbers satisfy $\frac{|b_1|\Delta\tau}{\Delta_1} + \frac{|b_2|\Delta\tau}{\Delta_2} \leq 1$.

Experiment settings. We set $b_1 = 0.8$, $b_2 = 0.4$, final time $T = 1$, and choose CFL such that $\frac{|b_1|\Delta\tau}{\Delta_1} + \frac{|b_2|\Delta\tau}{\Delta_2} = 0.6$. The initial condition u_0 is drawn from the periodic GRF prior (truncated to $N_{\text{KL}} = 64$) described in Section A.2.

B.3 Reaction–Diffusion (Allen–Cahn)

Model. We consider the Allen–Cahn reaction–diffusion equation on the periodic domain $\Omega = [0, 1]^2$:

$$\begin{cases} \partial_\tau u = D \Delta u + u - u^3, & \text{in } \Omega \times (0, \infty), \\ u(\cdot, 0) = u_0, & \text{in } \Omega, \end{cases}$$

where $D > 0$ is the diffusion coefficient and periodic boundary conditions are imposed.

Discretization. We use a uniform periodic $N \times N$ grid with spacings $\Delta_1 = \Delta_2 = \frac{1}{N}$, and denote the numerical solution by $u_{i,j}^n \approx u(\cdot, \tau^n)$ at time $\tau^n = n\Delta\tau$, with indices $i, j = 0, \dots, N-1$. We apply forward Euler in time and a five-point Laplacian (second-order central differences) in space:

$$u_{i,j}^{n+1} = u_{i,j}^n + \Delta\tau \left[D \left(\frac{u_{i+1,j}^n - 2u_{i,j}^n + u_{i-1,j}^n}{(\Delta_1)^2} + \frac{u_{i,j+1}^n - 2u_{i,j}^n + u_{i,j-1}^n}{(\Delta_2)^2} \right) + (u_{i,j}^n - (u_{i,j}^n)^3) \right],$$

where periodic boundary conditions are enforced by wrapping indices in each direction.

Stability (time step selection). A sufficient stability condition for the explicit diffusion term is

$$\Delta\tau \lesssim \text{CFL} \cdot \frac{\min(\Delta_1^2, \Delta_2^2)}{4D}.$$

Experiment settings. We set $T = 2$, $D = 10^{-3}$, and choose $\Delta\tau$ according to (B.3) with $\text{CFL} = 0.25$. The initial condition u_0 is drawn from the periodic GRF prior (truncated to $N_{\text{KL}} = 64$) described in Section A.2.

B.4 Navier–Stokes

Model. We consider the 2D incompressible Navier–Stokes equations in vorticity–streamfunction form on the periodic domain $\Omega = [0, 1]^2$:

$$\begin{cases} \partial_\tau u + \mathbf{q} \cdot \nabla u = \nu \Delta u + g, & \text{in } \Omega \times (0, \infty), \\ -\Delta \psi = u, & \text{in } \Omega, \\ \mathbf{q} = \nabla^\perp \psi := (\partial_2 \psi, -\partial_1 \psi), & \text{in } \Omega, \\ u(\cdot, 0) = u_0, & \text{in } \Omega, \end{cases}$$

where $\nu > 0$ is the viscosity, g is a prescribed forcing, and $\mathbf{q} = (q_1, q_2)$ is the (divergence-free) velocity field. Periodic boundary conditions are imposed. We fix the gauge by setting $\hat{\psi}(0) = 0$.

Discretization. We solve this equation using a Fourier pseudospectral method on an $N \times N$ grid. Fourier modes are indexed by $k = (k_1, k_2) \in \mathbb{Z}^2$ with $k_1, k_2 \in [-N/2, N/2)$, corresponding to the basis $e^{i2\pi k \cdot x}$ on $\Omega = [0, 1]^2$. Spatial derivatives are computed spectrally, e.g.

$$\widehat{\partial_1 \phi}(k) = i(2\pi k_1) \hat{\phi}(k), \quad \widehat{\partial_2 \phi}(k) = i(2\pi k_2) \hat{\phi}(k),$$

and the Laplacian has symbol

$$-\widehat{\Delta \phi}(k) = (2\pi)^2 |k|^2 \hat{\phi}(k) =: \lambda_k \hat{\phi}(k), \quad \lambda_k = (2\pi)^2 (k_1^2 + k_2^2).$$

At each time step, we obtain the streamfunction from

$$\hat{\psi}(k) = \frac{\hat{u}(k)}{\lambda_k}, \quad k \neq 0, \quad \hat{\psi}(0) = 0,$$

and recover the velocity in Fourier space by

$$\widehat{\mathbf{q}}(k) = i(2\pi) (k_2, -k_1) \hat{\psi}(k),$$

followed by inverse FFTs to physical space. The nonlinear advection is evaluated pseudospectrally: compute ∇u spectrally, form $F = \mathbf{q} \cdot \nabla u$ in physical space, then FFT back to obtain $(\widehat{\mathbf{q} \cdot \nabla u})$. We apply the standard 2/3 de-aliasing rule by zeroing modes with $|k_1| > \frac{N}{3}$ or $|k_2| > \frac{N}{3}$.

Time stepping uses an IMEX scheme with Crank–Nicolson for diffusion and explicit Euler for advection/forcing: for each nonzero mode $k \neq 0$,

$$\left(1 + \frac{1}{2}\nu\lambda_k\Delta\tau\right)\hat{u}^{n+1}(k) = \left(1 - \frac{1}{2}\nu\lambda_k\Delta\tau\right)\hat{u}^n(k) - \Delta\tau(\widehat{\mathbf{q} \cdot \nabla u})^n(k) + \Delta\tau\hat{g}(k),$$

where superscripts denote time levels $\tau^n = n\Delta\tau$.

Stability. Since diffusion is treated implicitly, stability is governed by the explicit advection. We enforce a convective CFL condition of the form

$$\Delta\tau \lesssim \frac{\text{CFL}}{\|\mathbf{q}\|_\infty 2\pi k_{\max}}, \quad 0 < \text{CFL} < 1,$$

where k_{\max} is the largest retained Fourier index (after de-aliasing). With the 2/3 rule, we take $k_{\max} = N/3$.

Experiment settings. We use a time-independent forcing

$$g(x_1, x_2) = A \left[\sin(2\pi(x_1 + x_2)) + \cos(2\pi(x_1 + x_2)) \right], \quad A = 0.1,$$

then set $\hat{g}(0, 0) = 0$ and apply the standard 2/3 de-aliasing rule to match the solver’s spectral truncation. The solver parameters are

$$\nu = 10^{-2}, \quad T = 0.2, \quad \Delta\tau = 10^{-3}.$$

The initial vorticity u_0 is sampled from the periodic GRF prior (truncated to $N_{\text{KL}} = 64$) described in Section A.2.

C Theory: noise geometry and transport regularity

In this appendix, we provide the underlying theoretical foundation on why we need a prior-aligned trace-class reference to realize the one-step map.

C.1 trace-class / anisotropic: Lipschitz-type regularity

We work in a function-space regime: let \mathcal{H} be a separable Hilbert space with norm $\|\cdot\|_{\mathcal{H}}$. In this section we explain why a prior-aligned trace-class (anisotropic) reference induces a resolution-robust geometry in which a globally Lipschitz one-step map is attainable.

We take the reference (latent) measure to be a centered Gaussian on \mathcal{H} ,

$$\rho = \gamma_A := \mathcal{N}(0, C),$$

where $C : \mathcal{H} \rightarrow \mathcal{H}$ is self-adjoint, nonnegative, and trace-class.

Assumption C.1 (Gaussian-tail target under the C -geometry). Fix y_{obs} and let $\pi(\cdot | y_{\text{obs}})$ be the target posterior on \mathcal{H} . Assume $\pi(\cdot | y_{\text{obs}})$ satisfies a Gaussian-tail condition under the C -geometry: there exists a (possibly degenerate) self-adjoint, nonnegative, trace-class operator $B : \mathcal{H} \rightarrow \mathcal{H}$ such that $\pi(\cdot | y_{\text{obs}}) \ll \mathcal{N}(0, B)$ and

$$\frac{d\pi(\cdot | y_{\text{obs}})}{d\mathcal{N}(0, B)}(x) \propto \exp(U(x)),$$

where U is twice Fréchet differentiable and satisfies the uniform bounds

$$\|\sqrt{C} \nabla U\|_{\infty} < \infty, \quad \|C \nabla^2 U\|_{\infty} < \infty.$$

Moreover, B and C induce the same Cameron–Martin space, and BC^{-1} and $B^{-1}C$ are bounded on this space.

Theorem C.2 (Dimension-free Lipschitz Föllmer velocity under Gaussian tails [23]). *Under Assumption C.1, the Föllmer velocity field $v(t, \cdot)$ associated with transporting $\rho = \mathcal{N}(0, C)$ to $\pi(\cdot | y_{\text{obs}})$ is globally Lipschitz and satisfies*

$$\text{Lip}(v(t, \cdot)) \leq L_0 t, \quad \forall t \in [0, 1],$$

where $L_0 > 0$ depends only on the Gaussian-tail parameters.

Remark C.3 (Function-space interpretation). Although Theorem C.2 is stated and proved in finite dimensions in [23], its Lipschitz bound involves constants that are independent of the ambient dimension. We therefore interpret it as a function-space stability statement.

Theorem C.4 (Averaged velocity is Lipschitz). *Assume Theorem C.2. Then average velocity $w(\cdot; r, t)$ for $0 \leq r \leq t \leq 1$ is globally Lipschitz and*

$$\text{Lip}(w(\cdot; r, t)) \leq \frac{1}{t-r} \int_r^t \text{Lip}(v(\tau, \cdot)) d\tau \leq L_0 \frac{t+r}{2}.$$

In particular, $\text{Lip}(w(\cdot; 0, 1)) \leq L_0/2$.

Corollary C.5 (Existence of a Lipschitz one-step map). *Define the one-step map*

$$\mathcal{T}(\xi; y_{\text{obs}}) := \xi - w(\xi; 0, 1), \quad \xi \in \mathcal{H}.$$

Under Assumption C.1, $\mathcal{T}(\cdot; y_{\text{obs}})$ is globally Lipschitz with

$$\text{Lip}(\mathcal{T}(\cdot; y_{\text{obs}})) \leq 1 + \frac{L_0}{2}.$$

Proof.

$$\begin{aligned} & \|\mathcal{T}(\xi_1; y_{\text{obs}}) - \mathcal{T}(\xi_2; y_{\text{obs}})\|_{\mathcal{H}} \\ &= \|(\xi_1 - \xi_2) - (w(\xi_1, 0, 1; y_{\text{obs}}) - w(\xi_2, 0, 1; y_{\text{obs}}))\|_{\mathcal{H}} \\ &\leq \left(1 + \frac{L_0}{2}\right) \|\xi_1 - \xi_2\|_{\mathcal{H}}. \end{aligned}$$

□

C.2 White vs trace-class: singularity / non-regular transport

This subsection highlights a function-space obstruction to using a discretization-level white reference. In typical PDE Bayesian inverse problem, the posterior $\pi(\cdot | y_{\text{obs}})$ is supported on the same Hilbert space \mathcal{H} as a trace-class Gaussian prior (and is often absolutely continuous with respect to it), whereas white noise does not take values in \mathcal{H} . This support mismatch rules out any regular (e.g., continuous/Lipschitz) deterministic one-step transport realized as a map $\mathcal{H} \rightarrow \mathcal{H}$.

Proposition C.6 (White reference vs. trace-class Gaussian are mutually singular). *Let \mathcal{H} be a separable Hilbert space with orthonormal basis $\{e_k\}_{k \geq 1}$. Fix $s > \frac{1}{2}$ and consider the distribution space \mathcal{H}^{-s} with norm*

$$\|x\|_{\mathcal{H}^{-s}}^2 := \sum_{k=1}^{\infty} k^{-2s} \langle x, e_k \rangle_{\mathcal{H}}^2.$$

Define the (formal) white reference latent by

$$\xi_{\text{W}} := \sum_{k=1}^{\infty} c_k e_k, \quad c_k \stackrel{\text{i.i.d.}}{\sim} \mathcal{N}(0, 1),$$

and denote its law on \mathcal{H}^{-s} by ρ_{W} (well-defined for $s > \frac{1}{2}$). Let $C : \mathcal{H} \rightarrow \mathcal{H}$ be self-adjoint, nonnegative, and trace-class with eigenpairs $C e_k = \lambda_k e_k$, $\lambda_k \geq 0$, $\sum_{k \geq 1} \lambda_k < \infty$. Define the trace-class (anisotropic) reference latent by

$$\xi_{\text{A}} := \sum_{k=1}^{\infty} \sqrt{\lambda_k} h_k e_k, \quad h_k \stackrel{\text{i.i.d.}}{\sim} \mathcal{N}(0, 1),$$

and denote its law on \mathcal{H}^{-s} by ρ_{A} . Then, as probability measures on \mathcal{H}^{-s} , $\rho_{\text{W}} \perp \rho_{\text{A}}$. Moreover, if a target measure π on \mathcal{H}^{-s} satisfies $\pi \ll \rho_{\text{A}}$ (in particular, $\pi(\mathcal{H}) = 1$), then $\rho_{\text{W}} \perp \pi$.

Proof. Consider the measurable set $\mathcal{H} \subset \mathcal{H}^{-s}$.

Step 1: $\rho_A(\mathcal{H}) = 1$. By trace-class,

$$\mathbb{E}\|\xi_A\|_{\mathcal{H}}^2 = \sum_{k=1}^{\infty} \lambda_k \mathbb{E}[h_k^2] = \sum_{k=1}^{\infty} \lambda_k < \infty.$$

Hence $\|\xi_A\|_{\mathcal{H}} < \infty$ almost surely and thus $\xi_A \in \mathcal{H}$ a.s., so $\rho_A(\mathcal{H}) = 1$.

Step 2: $\rho_W(\mathcal{H}) = 0$. If $\xi_W \in \mathcal{H}$, then $\|\xi_W\|_{\mathcal{H}}^2 = \sum_{k=1}^{\infty} c_k^2 < \infty$. However, by the strong law of large numbers,

$$\frac{1}{n} \sum_{k=1}^n c_k^2 \longrightarrow \mathbb{E}[c_1^2] = 1 \quad \text{a.s.},$$

which implies $\sum_{k=1}^{\infty} c_k^2 = \infty$ almost surely. Hence $\xi_W \notin \mathcal{H}$ a.s., so $\rho_W(\mathcal{H}) = 0$.

Therefore $\rho_W(\mathcal{H}) = 0$ and $\rho_A(\mathcal{H}) = 1$, which yields $\rho_W \perp \rho_A$. Finally, if $\pi \ll \rho_A$ and $\rho_A(\mathcal{H}) = 1$, then $\pi(\mathcal{H}) = 1$, while $\rho_W(\mathcal{H}) = 0$; hence $\rho_W \perp \pi$. \square

In our main setting, $\pi(\cdot | y_{\text{obs}})$ is absolutely continuous with respect to the trace-class prior as in (2), so $\pi(\cdot | y_{\text{obs}}) \ll \rho_A$ and $\pi(\mathcal{H} | y_{\text{obs}}) = 1$. Proposition C.6 therefore shows that a white reference ρ_W is incompatible with a regular deterministic one-step transport $T : \mathcal{H} \rightarrow \mathcal{H}$ in the function-space regime, which motivates the prior-aligned trace-class choice $\rho = \rho_A$.

Remark C.7 (Finite-dimensional discretizations are not singular). On any fixed finite discretization, nondegenerate Gaussians $\mathcal{N}(0, I_d)$ and $\mathcal{N}(0, C_d)$ (with $C_d \succ 0$) are mutually absolutely continuous. The above singularity is a genuinely infinite-dimensional phenomenon.

The next example makes the above support mismatch explicit by exhibiting a concrete pushforward on \mathcal{H}^{-s} .

Example C.8 (A pushforward exists on \mathcal{H}^{-s} but is singular on \mathcal{H}). Let ρ_W and ρ_A be as in Proposition C.6. Define the linear map on the distribution space \mathcal{H}^{-s} by

$$\mathcal{T} : \mathcal{H}^{-s} \rightarrow \mathcal{H}^{-s}, \quad \mathcal{T}(\xi) = C^{1/2}\xi,$$

where $C^{1/2}$ acts diagonally in the basis $\{e_k\}$. Then $\mathcal{T}_{\#}\rho_W = \rho_A$ as probability measures on \mathcal{H}^{-s} . However, this pushforward is *singular* at the level of \mathcal{H} :

$$\rho_W(\mathcal{H}) = 0, \quad (\mathcal{T}_{\#}\rho_W)(\mathcal{H}) = \rho_A(\mathcal{H}) = 1.$$

Thus \mathcal{T} maps ρ_W -almost every input (which lies outside \mathcal{H}) to an \mathcal{H} -valued output, and cannot be realized as a continuous or Lipschitz map $\mathcal{H} \rightarrow \mathcal{H}$.

D Alternative model structures

In this appendix, we report training results for a range of model variants. For the transport parameterization, we additionally consider an Encode–Decode mechanism. For the operator backbone, we also evaluate PODNO and UNet architectures. After that, we include Improved Mean Flows [10], a recently proposed variant of Mean Flows. Finally, we consider a multistep diffusion model.

Algorithm 3 Training: Encode–Decode Mean Flows

Input: Training pairs $\{(x^{(i)}, y_{\text{obs}}^{(i)})\}_{i=1}^{N_{\text{train}}}$; reference/latent measure ρ ; normalizers $\mathcal{E}_x, \mathcal{E}_y$.

Preprocessing:

Estimate normalization statistics (μ_x, σ_x) and (μ_y, σ_y) from the training set, and define encoders $\tilde{y}_{\text{obs}} = \mathcal{E}_y(y_{\text{obs}})$ in (5) and $\tilde{x} = \mathcal{E}_x(x)$ in (6).

repeat

Sample a mini-batch (x, y_{obs}) from the training set.

Encode $\tilde{x} = \mathcal{E}_x(x)$ and $\tilde{y}_{\text{obs}} = \mathcal{E}_y(y_{\text{obs}})$.

Sample $\xi \sim \rho$ independently.

Encode latent: $\tilde{\xi} = \mathcal{E}_x(\xi)$.

Sample (r, t) with $0 \leq r \leq t \leq 1$.

Form the interpolation state:

$$z_t = (1 - t)\tilde{x} + t\tilde{\xi}, \quad v := \tilde{\xi} - \tilde{x}.$$

Set the (stop-gradient) Mean Flows target:

$$w_{\text{tgt}} := v - (t - r) \text{JVP}_{(z,r,t)}(w_\theta; (v, 0, 1)).$$

Decode to physical space:

$$\hat{w}_\theta := D\mathcal{E}_x^{-1}w_\theta(z_t, r, t; \tilde{y}_{\text{obs}}), \quad \hat{w}_{\text{tgt}} := D\mathcal{E}_x^{-1}w_{\text{tgt}},$$

where $D\mathcal{E}_x^{-1} = I$ for $\rho = \gamma$, and $D\mathcal{E}_x^{-1} = \text{diag}(\sigma_x)$ for $\rho = \rho_W$.

Update θ by minimizing the physical-space MSE loss

$$\|\hat{w}_\theta - \text{sg}(\hat{w}_{\text{tgt}})\|^2.$$

until convergence

Output: trained parameters $\hat{\theta}$.

Algorithm 4 Sampling: One-step Encode–Decode Mean Flows

Input: Observation y_{obs} ; trained parameter $\hat{\theta}$; reference/latent measure ρ ; normalizers $\mathcal{E}_x, \mathcal{E}_y$.

Encode observation $\tilde{y}_{\text{obs}} = \mathcal{E}_y(y_{\text{obs}})$.

Sample reference: $\xi \sim \rho$.

Encode reference: $\tilde{\xi} = \mathcal{E}_x(\xi)$.

Generate an encoded sample:

$$\tilde{x} = \tilde{\xi} - w_{\hat{\theta}}(\tilde{\xi}, 0, 1; \tilde{y}_{\text{obs}}).$$

Decode *state* to physical space:

$$x = \mathcal{E}_x^{-1}(\tilde{x}).$$

Output: Posterior sample x .

Encode–decode model Algorithms 3–4 implement an *encode–decode* variant: the network takes encoded states as input and predicts velocities in the encoded coordinates, while the loss is computed after mapping the prediction back to physical space. This distinction is typically benign for trace-class (anisotropic) references, but becomes critical under a white-noise reference. Empirically, Table 3 shows that for Advection, Reaction–Diffusion, and Navier–Stokes, Encode–Decode with a white reference produces posterior samples and statistics that deviate substantially from the ground truth.

We attribute this behavior to the J^*J -weighted regression as shown in (9) and (10). This

Table 3: Evaluation results across different inverse problems and reference types, using an Encode-Decode Mean Flows model with an FNO backbone.

Dataset	Reference	$\epsilon_{\mu}^{\text{eval}}$	$\epsilon_{\sigma}^{\text{eval}}$
Darcy	Anisotropic	5.52×10^{-2}	4.76×10^{-2}
	White	6.19×10^{-2}	4.31×10^{-2}
Advection	Anisotropic	8.09×10^{-2}	2.09×10^{-1}
	White	1.36×10^1	5.11×10^0
Reaction-Diffusion	Anisotropic	8.57×10^{-2}	3.15×10^{-1}
	White	1.73×10^1	7.72×10^0
Navier-Stokes	Anisotropic	6.74×10^{-2}	2.92×10^{-1}
	White	1.15×10^0	6.31×10^0

yields an ill-conditioned optimization landscape—manifested by large gradient/Jacobian norms—and produces pronounced high-frequency deviations in the generated samples (cf. the full-KL identity experiment in Figure 1). In contrast, for trace-class (anisotropic) references, the high-frequency energy decays, rendering the induced metric more robust under mesh refinement and making the regression problem substantially better conditioned.

D.1 Operator Backbone Variants: PODNO

Table 4: Evaluation results across different inverse problems and reference types, using an Encode-only Mean Flows model with a PODNO backbone.

Dataset	Reference	$\epsilon_{\mu}^{\text{eval}}$	$\epsilon_{\sigma}^{\text{eval}}$
Darcy	Anisotropic	5.55×10^{-2}	5.45×10^{-2}
	White	7.56×10^{-2}	4.37×10^{-2}
Advection	Anisotropic	6.36×10^{-2}	3.76×10^{-2}
	White	1.43×10^{-1}	5.08×10^{-2}
Reaction-Diffusion	Anisotropic	7.23×10^{-2}	7.94×10^{-2}
	White	8.08×10^{-2}	7.85×10^{-2}
Navier-Stokes	Anisotropic	5.91×10^{-2}	5.50×10^{-2}
	White	8.08×10^{-2}	5.52×10^{-2}

The proposed one-step Mean Flows framework is agnostic to the choice of operator backbone. Beyond FNO, we also evaluated Proper Orthogonal Decomposition Neural Operators (PODNO) [4] under the same Mean Flows formulation and with matched parameter budgets: we use 288 POD modes for PODNO and 12 Fourier modes for FNO, yielding 1.2×10^8 parameters in both cases.

Across all benchmarks, PODNO achieves posterior accuracy comparable to FNO while offering significant computational advantages. By projecting the dynamics onto a low-dimensional POD basis, PODNO reduces the cost of online spectral operations and leads to approximately a two-fold speedup in training, without degrading posterior mean or uncertainty estimates.

These results indicate that the proposed framework is compatible with a range of operator-learning architectures. Designing operator backbones that are both computationally efficient and well-conditioned for probabilistic transport remains an important direction for future work.

D.2 UNet Backbone: Limitations for Function-Space Transport

We also tested UNet-based backbones within the same one-step Mean Flows framework. While UNets are widely used in diffusion models for image generation, the primary limitation is

Table 5: Evaluation results across different inverse problems and reference types, using an Encode-only Mean Flows model with a U-Net backbone.

Dataset	Reference	$\epsilon_\mu^{\text{eval}}$	$\epsilon_\sigma^{\text{eval}}$
Darcy	Anisotropic	1.02×10^{-1}	1.48×10^{-1}
	White	1.41×10^{-1}	1.02×10^{-1}
Advection	Anisotropic	7.34×10^{-2}	1.37×10^{-1}
	White	2.04×10^{-1}	1.04×10^{-1}
Reaction-Diffusion	Anisotropic	9.17×10^{-2}	2.04×10^{-1}
	White	1.44×10^{-1}	1.44×10^{-1}
Navier-Stokes	Anisotropic	1.06×10^{-1}	1.31×10^{-1}
	White	1.29×10^{-1}	9.98×10^{-2}

structural. UNet is a grid-dependent convolutional architecture, designed to exploit local spatial correlations at a fixed resolution. In contrast, the transport map in Bayesian PDE inverse problems is inherently an operator acting on function spaces, with global and nonlocal dependence induced by the forward PDE and the observation operator.

As a consequence, UNets require substantially more parameters (in our setting, 1.7×10^9 compared to 1.2×10^8), yet still deliver inferior performance and struggle to represent resolution-independent transport maps. In practice, this manifests as slower convergence and poorer posterior uncertainty estimates compared to neural operator backbones such as FNO or PODNO.

D.3 Improved Mean Flows model

Algorithm 5 Training: Encode-only Improved Mean Flows (iMF)

Input: Training pairs $\{(x^{(i)}, y_{\text{obs}}^{(i)})\}_{i=1}^{N_{\text{train}}}$; reference/latent measure ρ (prior-aligned $\rho = \gamma$ in our main setting).

Preprocessing:

Estimate normalization statistics (μ_x, σ_x) and (μ_y, σ_y) from the training set, and define encoders $\tilde{y}_{\text{obs}} = \mathcal{E}_y(y_{\text{obs}})$ in (5) and $\tilde{x} = \mathcal{E}_x(x)$ in (6).

Initialize: network parameters θ .

repeat

Sample a mini-batch (x, y_{obs}) from the training set.

Encode $\tilde{x} = \mathcal{E}_x(x)$ and $\tilde{y}_{\text{obs}} = \mathcal{E}_y(y_{\text{obs}})$.

Sample $\xi \sim \rho$ independently.

Sample (r, t) with $0 \leq r \leq t \leq 1$.

Form the interpolation state

$$z_t = (1 - t)\tilde{x} + t\xi, \quad v := \frac{d}{dt}z_t = \xi - \tilde{x}.$$

Compute surrogate direction

$$v_\theta(z_t, t; \tilde{y}_{\text{obs}}) := w_\theta(z_t, t, t; \tilde{y}_{\text{obs}}).$$

Predict

$$V_\theta := w_\theta(z_t, r, t; \tilde{y}_{\text{obs}}) + (t - r) \text{sg}\left(\text{JVP}_{(z,r,t)}(w_\theta; (v_\theta, 0, 1))\right).$$

Update θ by minimizing $\|V_\theta - v\|^2$ (encoded-space MSE).

until convergence

Output: trained parameters $\hat{\theta}$.

Algorithm 6 Sampling: One-step Encode-only improved Mean Flows (iMF)

Input: Observation y_{obs} ; trained parameters $\hat{\theta}$; reference/latent measure ρ ; normalizers $\mathcal{E}_x, \mathcal{E}_y$.
Encode observation $\tilde{y}_{\text{obs}} = \mathcal{E}_y(y_{\text{obs}})$.

Sample $\xi \sim \rho$.

Generate an encoded sample:

$$\tilde{x} = \xi - w_{\hat{\theta}}(\xi, 0, 1; \tilde{y}_{\text{obs}}).$$

Decode to physical space: $x = \mathcal{E}_x^{-1}(\tilde{x})$.

Output: Posterior sample x .

Table 6: Evaluation results across different inverse problems and reference types, using an encode-only improved Mean Flows model with an FNO backbone.

Dataset	Reference	$\epsilon_{\mu}^{\text{eval}}$	$\epsilon_{\sigma}^{\text{eval}}$
Darcy	Anisotropic	5.43×10^{-2}	6.16×10^{-2}
	White	2.80×10^9	3.14×10^9
Advection	Anisotropic	7.19×10^{-2}	5.05×10^{-2}
	White	1.11×10^{10}	1.91×10^5
Reaction-Diffusion	Anisotropic	8.23×10^{-2}	9.64×10^{-2}
	White	2.16×10^{10}	6.14×10^5
Navier–Stokes	Anisotropic	6.86×10^{-2}	6.52×10^{-2}
	White	1.71×10^{10}	3.50×10^5

We additionally test *Improved Mean Flows* (iMF) [10], which augments Mean Flows training with an explicit total-derivative (JVP) correction in a training-time composite predictor. Let

$$z_t = (1 - t)\tilde{x} + t\xi, \quad v := \frac{d}{dt}z_t = \xi - \tilde{x},$$

and use the boundary-trick surrogate direction

$$v_{\theta}(z_t, t; \tilde{y}_{\text{obs}}) := w_{\theta}(z_t, t, t; \tilde{y}_{\text{obs}}).$$

iMF forms

$$V_{\theta} := w_{\theta}(z_t, r, t; \tilde{y}_{\text{obs}}) + (t - r) \text{sg}\left(\text{JVP}_{(z,r,t)}(w_{\theta}; (v_{\theta}, 0, 1))\right), \quad (15)$$

which is not an independent network and regresses V_{θ} to the instantaneous target v :

$$\mathcal{L}_{\text{iMF}}(\theta) = \mathbb{E}\|V_{\theta} - v\|^2.$$

Here $\text{JVP}_{(z,r,t)}(w_{\theta}; (v_{\theta}, 0, 1))$ denotes the directional derivative of $(z, r, t) \mapsto w_{\theta}(z, r, t; \tilde{y}_{\text{obs}})$ along $(v_{\theta}, 0, 1)$, i.e.,

$$\text{JVP}_{(z,r,t)}(w_{\theta}; (v_{\theta}, 0, 1)) = D_z w_{\theta}(z_t, r, t; \tilde{y}_{\text{obs}})[v_{\theta}] + \partial_t w_{\theta}(z_t, r, t; \tilde{y}_{\text{obs}}),$$

where $D_z w_{\theta}[\cdot]$ denotes the Jacobian–vector product with respect to z .

Table 6 shows a consistent pattern across all PDE inverse problems. With a prior-aligned trace-class (anisotropic) reference, iMF trains stably and yields accurate posterior means and standard deviations. With a white-noise reference, training can become numerically unstable (loss blow-up or ∞) and posterior statistics deteriorate. This is consistent with the iMF correction being evaluated along the model-dependent direction v_{θ} : under white-noise references, resolution-sensitive high-frequency components can amplify $D_z w_{\theta}[v_{\theta}]$ and hence the correction term in (15), whereas a trace-class reference suppresses these directions and stabilizes the JVP correction.

Table 7: Evaluation results across different inverse problems and reference types, using an Encode-only multistep Diffusion model with an FNO backbone.

Dataset	Reference	$\epsilon_{\mu}^{\text{eval}}$	$\epsilon_{\sigma}^{\text{eval}}$
Darcy	Anisotropic	1.08×10^{-1}	7.00×10^{-2}
	White	1.19×10^{-1}	7.71×10^{-2}
Advection	Anisotropic	9.90×10^{-2}	4.30×10^{-2}
	White	2.99×10^{-1}	8.24×10^{-2}
Reaction-Diffusion	Anisotropic	1.08×10^{-1}	1.02×10^{-1}
	White	1.16×10^{-1}	9.21×10^{-2}
Navier–Stokes	Anisotropic	9.97×10^{-2}	8.08×10^{-2}
	White	1.09×10^{-1}	7.63×10^{-2}

D.4 Multistep diffusion model

We additionally include a multistep diffusion-style paradigm to quantify both sampling efficiency and posterior accuracy. This model is trained with a denoising (CEM/MMSE) objective and is therefore compared with our one-step Mean Flow at the *paradigm* level. To isolate this paradigm-level difference, we match all other components—conditioning, operator backbone, and reference geometry—so that observed gaps are attributable primarily to the multistep denoising objective together with the repeated application of the reverse chain.

Concretely, the multistep model is trained as a conditional denoiser that regresses the clean state from a noisy intermediate,

$$x_{\theta}(z_t, t; \tilde{y}_{\text{obs}}) \approx \mathbb{E}[x|z_t, t, \tilde{y}_{\text{obs}}], \quad \min_{\theta} \mathbb{E}[\|x_{\theta}(z_t, t; \tilde{y}_{\text{obs}}) - x\|^2],$$

where $z_t = \alpha(t)x + \beta(t)\xi$ is produced by the forward process. We use the standard VP-style parameterization $\alpha(t) = e^{-t/2}$ and $\beta(t) = \sqrt{1 - e^{-t}}$.

Multistep sampling is substantially more expensive: each reverse update requires an additional forward pass of the conditional operator network, so the generation time scales approximately linearly with the number of steps N_T . In our main evaluation with $N_T = 320$, this leads to a markedly larger wall-clock generation time than one-step sampling (Table 1).

While multistep diffusion can be more expressive in principle, it requires a denoiser that is well calibrated across many noise levels and is repeatedly applied during sampling. In our function-space PDE inverse problems, we found that, across a reasonable range of step counts and standard schedule choices, the multistep baseline consistently underperforms our one-step model in posterior statistics, while incurring a much higher sampling cost. By contrast, one-step Mean Flow learns a single conditional transport map and is evaluated only once at test time, achieving both higher accuracy and much faster sampling in our setup.

E Notation and Network/Training Settings

Table 8: Notation.

Symbol	Description
Ω	Spatial domain
w	Averaged velocity field
v	Instantaneous velocity field
\mathcal{T}	Transport map (one-step map from prior to posterior)
T	PDE final time (observation time)
\mathcal{H}	Separable Hilbert space
m	Number of observation points
z_t	Interpolated/noised state at time t
γ	Prior distribution (reference measure)
ρ	Reference distribution, ρ_A/ρ_W for anisotropic/white reference
π	Posterior distribution (target measure)
\mathcal{G}	Forward operator
ψ	Hidden state in the conditional neural operator
η	Measurement noise
y_{obs}	Observation vector
θ	Network weights (trainable parameters)
$\hat{\theta}$	Trained parameters selected at convergence / by early stopping (used at inference)
s	Sobolev regularity exponent defining the distribution space \mathcal{H}^{-s}
N	Mesh resolution parameter, $N \times N$ for 2D problems
r	Start time of the Mean-Flow interpolation (source/corruption level)
t	End time of the Mean-Flow interpolation (target/corruption level)
μ_{true}	Ground-truth (reference) posterior mean
σ_{true}	Ground-truth (reference) posterior pointwise standard deviation
$\mu_{\text{pred}}(y_{\text{obs}})$	Predicted posterior mean (from the learned model)
$\sigma_{\text{pred}}(y_{\text{obs}})$	Predicted posterior pointwise standard deviation (from the learned model)
$\epsilon_{\mu}^{\text{eval}}$	Relative $L^2(\Omega)$ error of posterior mean
$\epsilon_{\sigma}^{\text{eval}}$	Relative $L^2(\Omega)$ error of posterior standard deviation

Table 9: Network architecture and training hyperparameters.

Setting	Symbol	Value
FNO Fourier modes	K	12
PODNO POD modes	K_{POD}	288
FNO/PODNO layers	L	4
Network width	N_{width}	96
Learning rate	ν_{learning}	10^{-4}
Flow ratio	ν_{flow}	0.25
Batch size	N_{batch}	20
Epochs	N_{epoch}	1000
Training size	N_{train}	10000
Number of samples for $\epsilon_{\mu}^{\text{eval}}/\epsilon_{\sigma}^{\text{eval}}$ estimation	N_{eval}	1000
Time sampling	(r, t)	Uniform in $[0, 1]$
Resolution (Identity, Darcy)	N^2	65×65
Resolution (Advection, Reaction-Diffusion, Navier-Stokes)	N^2	64×64
Observation count (Identity, Darcy)	m	49
Observation count (Advection, Reaction-Diffusion, Navier-Stokes)	m	64
KL modes (anisotropic noise, Identity)	n_{KL}	$65^2 - 1$
KL modes (anisotropic noise, PDE datasets)	n_{KL}	64